Information Sciences 246 (2013) 1–27

Contents lists available at SciVerse ScienceDirect

Information Sciences

journal homepage: www.elsevier.com/locate/ins

A constraint propagation approach to structural model based image segmentation and recognition

Olivier Nempont [a,c], Jamal Atif [b], Isabelle Bloch [a,*]

[a] Institut Mines-Telecom, Telecom ParisTech, CNRS LTCI, 46 rue Barrault, 75013 Paris, France
[b] TAO INRIA, CNRS, LRI – Paris-Sud University, 91405 Orsay Cedex, France
[c] Philips Research, 33 rue de Verdun, 92150 Suresnes, France

ARTICLE INFO

Article history:
Received 11 January 2012
Received in revised form 11 April 2013
Accepted 16 May 2013
Available online 28 May 2013

Keywords:
Image interpretation
Constraint satisfaction
Fuzzy set
Structural model

ABSTRACT

The interpretation of complex scenes in images requires knowledge regarding the objects in the scene and their spatial arrangement. We propose a method for simultaneously segmenting and recognizing objects in images, that is based on a structural representation of the scene and a constraint propagation method. The structural model is a graph representing the objects in the scene, their appearance and their spatial relations, represented by fuzzy models. The proposed solver is a novel global method that assigns spatial regions to the objects according to the relations in the structural model. We propose to progressively reduce the solution domain by excluding assignments that are inconsistent with a constraint network derived from the structural model. The final segmentation of each object is then performed as a minimal surface extraction. The contributions of this paper are illustrated through the example of brain structure recognition in magnetic resonance images.

1. Introduction

The interpretation of complex scenes in images often requires (or can benefit from) a model of the scene. This model may provide information regarding the objects contained in the scene, as well as their spatial arrangement. The spatial layout information is often crucial for differentiating among objects with similar appearances in the images, or disambiguating complex cases. Examples occur in many domains, including medical imaging, in which structural knowledge can help in the interpretation of the images. In magnetic resonance imaging (MRI), for instance, radiometry is often insufficient for recognizing individual anatomical structures, and their relative spatial configuration provides an important input into the recognition process [17]. Other examples occur in aerial and satellite imaging, robot vision, and video sequence interpretation, among other fields. In this paper, we address the image interpretation problem as a joint problem of image segmentation and object recognition, based on structural information. Although the focus of the paper is methodological and theoretical, remaining as generic as possible, we illustrate the proposed method through the concrete example of 3D brain MRI interpretation.

Graphs are often used to represent the structural information in image interpretation, where the vertices represent objects or image regions (and may carry attributes such as their shapes, sizes, and colors or gray levels), and the edges carry the structural information, such as the spatial relations among objects, or radiometric contrasts between regions. Although this type of representation has become popular in the last 30 years [18], a number of open problems remain in its efficient imple-

* Corresponding author.
E-mail address: isabelle.bloch@telecom-paristech.fr (I. Bloch).

0020-0255/$ - see front matter © 2013 Elsevier Inc. All rights reserved.
http://dx.doi.org/10.1016/j.ins.2013.05.030

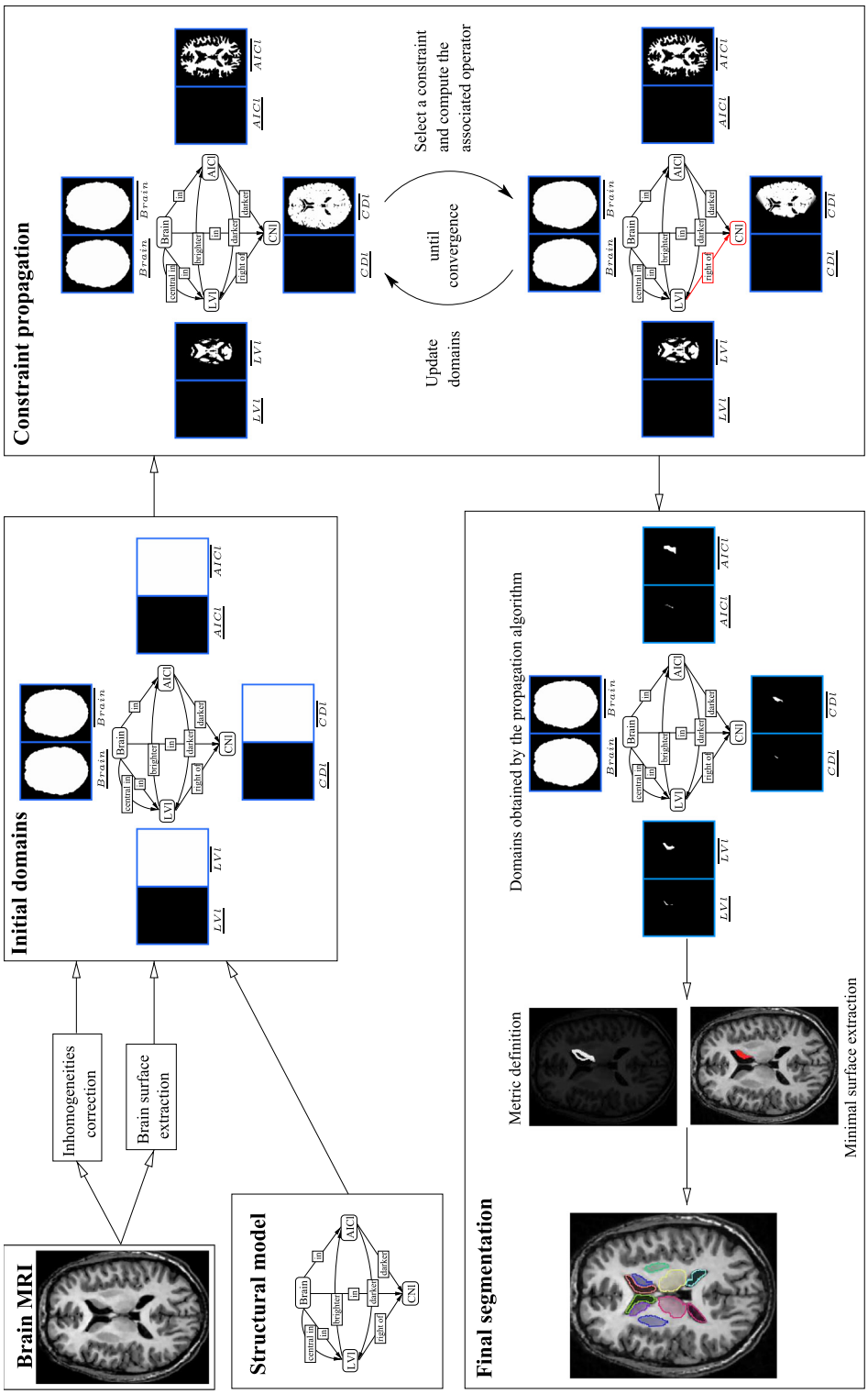

Fig. 1. Overview of the proposed approach for the brain structures example. For instance, the solution space of the left caudate nucleus (*CNl*) is reduced based on the constraint that "the left caudate nucleus (*CNl*) is exterior (i.e. to the right in the image) to the left lateral ventricle (*LVl*)".

mentation. In one type of approach, the graph is derived from the image itself, based on a preliminary segmentation into homogeneous regions, and the recognition problem is expressed as a graph matching problem between the image and model

graphs, which is an annotation problem. However this scheme often requires solving complex combinatorial problems [18]. Improvements can be achieved by suppressing iteratively inconsistent annotations using a constraint propagation procedure, as proposed e.g. in [50,58] for simple geometrical figures or in [31,56] for the annotation of image segmentations. However, the constraint propagation procedure does not guarantee a unique annotation. Moreover, all of these approaches assume a correct initial segmentation of the image. However, the segmentation problem is a known challenge in image processing, to which no universal solution exists. The segmentation is usually imperfect, and no isomorphism exists between the graphs being matched. An inexact matching must then be found, for instance by allowing several image regions to be assigned to one model vertex or by relaxing the notion of morphism to that of fuzzy morphism [14,46]. For example, previous studies [19,20] employ an over-segmentation of the image, which is easier to obtain. A model structure (i.e. a graph vertex) is then explicitly associated with a set of regions, and the recognition problem is expressed as a constraint satisfaction problem. To overcome the complexity issue, a weaker version of the model relations (encoded in the edges) is considered, and the problem is solved using a modified AC-4 propagation algorithm [38]. Other recent approaches, still based on a preliminary segmentation, have revisited the grammatical approach to pattern recognition [48,57,65,66], or employed probabilistic models [27,61,64] or ontologies [29,44].

To deal with the difficulty of obtaining a relevant segmentation, the segmentation and recognition can also be performed simultaneously. For instance, in the method proposed in previous studies [8,17], the structures of interest are segmented and recognized sequentially, in a pre-calculated order [23]. The structures that are easier to segment are considered first and adopted as reference objects. The spatial relations to these structures are encoded in the structural model and are used as constraints to guide the segmentation and recognition of other structures. Due to the sequential nature of the process, the errors are potentially propagated. Backtracking may then be needed, as proposed in [23].

To overcome the problems raised by sequential approaches while avoiding the need for an initial segmentation, we propose an original method that still employs a structural model, but solves the problem in a global fashion. Our definition of a solution is the assignment of a spatial region to each model object, in a way that satisfies the constraints expressed in the model. We propose a progressive reduction of the solution domain for all objects by excluding assignments that are inconsistent with the structural model. Constraint networks constitute an appropriate framework for both the formalization of the problem and the optimization. An original feature of the proposed approach is that the regions are not predetermined, but are instead constructed during the reduction process. The image segmentation and recognition algorithm therefore differs from an annotation procedure, and no prior segmentation of the image into meaningful or homogeneous regions is required. This feature overcomes the limitations of many previous approaches (such as [19,20]). More precisely, a constraint network is constructed from the structural model, and a propagation algorithm is then designed to reduce the search space. Finally, an approximate solution is extracted from the reduced search space. This procedure is illustrated in Fig. 1, using the interpretation of a brain MRI as an example. Once the propagation process terminates, the solution space is typically reduced substantially for all of the model structures. The final segmentation and recognition results can then be obtained using any segmentation method that is constrained by this solution space.

In Section 2, we summarize the main components of the structural model. Some preliminaries on constraint networks are reviewed in Section 3. The novel contributions of this paper are described in Sections 4 and 5, extending our preliminary work in [42]. We describe the expression of the constraints in detail, and propose propagators that are adapted to each type of constraint. The power and tractability of the proposed approach are illustrated using both a synthetic example and a real-world example, in which anatomical brain structures are recognized in MR images (Section 6).

2. Graphical structural model

The structural model used in this paper was developed previously in [8,17,29]. The model consists of a graph in which the vertices represent objects, and the edges encode structural relations and relations describing the radiometric contrasts. Both the vertices and the edges have attributes. As an original feature of this model, spatial relations are represented using fuzzy models [5], which define the semantics of the relations, and enable us to link abstract concepts to spatial representations [29]. This approach helps filling the semantic gap between symbolic information and the visual percepts that are extracted from the images.

We now describe this model in the context of the brain structures example (these structures are then the objects to be recognized in a medical image). Brain anatomy is commonly described in a hierarchical fashion [10,35], and can be formalized using ontologies. One of these ontologies is the Foundational Model of Anatomy (FMA) [51]. In addition, the spatial organization of the anatomical structures is a major component of linguistic descriptions of the brain anatomy [28,60], and has therefore been added to the existing ontology [29]. Based on these sources of knowledge, an attributed hierarchical graph describing the brain anatomy has been proposed in [16,30]. The relations in this model include spatial relations, such as topological, distance and direction relations, according to the hierarchy of spatial relations proposed in [32], as well as radiometric relations. Although the radiometry of each structure in an MR image may vary depending on the acquisition, the contrast between structures is quite robust and stable for a given acquisition protocol.

This model is particularly relevant because the overall structure of the brain is quite stable, while the shapes and sizes of the individual structures are prone to substantial variability. The fuzziness of the representations makes it possible to handle

the imprecision and limited variability of the relations, even in pathological cases. Brain imaging is therefore an ideal example through which to illustrate the proposed structural approach.

3. Some preliminaries on constraint networks

A large body of research has been dedicated to the topic of constraint networks, particularly in artificial intelligence and operational research, for problems such as planning, recognition of segmented images [19,50,58], and image segmentation [34]. In this paper, we demonstrate the feasibility of model-based image interpretation without any preliminary segmentation, using constraint networks.

In this section, the main definitions and notations adopted in the sequel of this paper are provided. Comprehensive surveys of constraint networks and constraint propagation can be found for instance in [3,52].

3.1. General definitions

A constraint network is defined by a triplet $N = \langle \chi, \mathcal{D}, \mathcal{C} \rangle$ where: $\chi = \{x_1, \ldots, x_n\}$ is the set of *variables* in the problem, and $\mathcal{D}$ is the set of *domains* associated with those variables. Each variable $x_i \in \chi$ takes values in the domain $\mathcal{D}(x_i)$, and $\mathcal{C}$ is a set of *constraints*. Each constraint $C \in \mathcal{C}$ is a relation defined on a set of variables $vars(C)$, such that $vars(C) \subseteq \chi$. A relation is then a subset of the Cartesian product of the domains associated with the variables $vars(C)$.

We denote by $I = \{(x_1, v_1), \ldots, (x_k, v_k)\}$ an instantiation on the variables $Y = \{x_1, \ldots, x_k\} \subseteq \chi$. An instantiation I is valid if $\forall x_i \in Y,\ v_i \in \mathcal{D}(x_i)$, the domain associated with x_i. For $Y' \subseteq Y$, $I[Y']$ denotes the projection of I onto Y'. An instantiation I satisfies a constraint C such that $vars(C) \subseteq Y$ if $I[vars(C)] \in C$, and I is locally consistent if I is valid and for each constraint $C \in \mathcal{C}$ such that $vars(C) \subseteq Y$, I satisfies C.

A solution of the constraint network N is a locally consistent instantiation I on χ. We denote the set of solutions of N by $sol(N)$. A constraint network is said to be satisfiable if it has at least one solution.

3.2. Constraint propagation

Various efficient backtracking algorithms [26,52] have been proposed for solving constraint satisfaction problems. However, many problems cannot be solved using these algorithms because of the complexity of the problem. To simplify a problem, a constraint propagation algorithm can be applied first. It can be used to iteratively transform an initial constraint network N into a simpler network N' with the same solutions by: (i) reducing the domains of the variables, and (ii) inferring new constraints.

Let $N = \langle \chi, \mathcal{D}, \mathcal{C} \rangle$. The set $\mathcal{P}_{ND}$ of all domain-based tightenings of N is the set of networks $\{N' = \langle \chi, \mathcal{D}', \mathcal{C} \rangle\}$ such that $\mathcal{D}' \subseteq \mathcal{D}$. We denote the partial ordering on $\mathcal{P}_{ND}$ associated with the domain inclusion relation by $\leqslant_N$. The set $\mathcal{P}^{sol}_{ND}$ is the subset of networks in $\mathcal{P}_{ND}$ that present the same solutions as N, i.e. $\forall N' \in \mathcal{P}^{sol}_{ND},\ sol(N') = sol(N)$. $\mathcal{P}^{sol}_{ND}$ has a least element denoted by G_{ND}, whose domains contain only values that belong to a solution. Because the computation of G_{ND} is NP-hard, domain-based constraint propagation is used to determine the smallest possible element of $\mathcal{P}^{sol}_{ND}$ in polynomial time. This procedure iteratively removes values that cannot belong to a solution by, for instance, applying propagators. A propagator f is an operator associated with a constraint $C \in \mathcal{C}$. It tightens the domains $(\forall N' \in \mathcal{P}_{ND}, f(N') \in \mathcal{P}_{N'D})$ regardless of the other constraints. A propagator f is *correct* if $\forall N' \in \mathcal{P}^{sol}_{ND},\ f(N') \in \mathcal{P}^{sol}_{N'D}$, *increasing* if $\forall N_1, N_2 \in \mathcal{P}_{ND},\ N_1 \leqslant_N N_2 \Rightarrow f(N_1) \leqslant_N f(N_2)$, and *idempotent* if $\forall N' \in \mathcal{P}_{ND},\ f(f(N')) = f(N')$. A constraint propagation process that iteratively applies a set of propagators ends when no propagator can reduce a domain. If the propagators are increasing, which is generally the case, then the result does not depend on the order of application of the propagators, and is called the least fixed point. These properties are therefore important, and will be checked for the proposed propagators.

The propagators are generally associated with a notion of local consistency. For instance, an arc consistent [36] propagator associated with a constraint C removes all values that are not arc consistent with C with respect to the current domains. The constraint C is then arc consistent in $\mathcal{D}$. Certain notions of local consistency, such as path consistency [39], are more restrictive, whereas notions such as bound consistency are more permissive and lead to cheaper propagators. Several definitions of bound consistency have been proposed [3,15]. For instance for variables taking values in $\mathbb{Z}$, $\mathcal{D}$ is *bounds*(Z)-consistent with the constraint C if for each x_i in $vars(C)$, the bounds of the domain, $\inf_{v_i \in \mathcal{D}(x_i)}(v_i)$ and $\sup_{v_i \in \mathcal{D}(x_i)}(v_i)$, have a support on C in $\mathcal{D}^I$, where $\mathcal{D}^I$ are the domains represented as intervals: $\forall x_i \in \chi,\ \mathcal{D}^I(x_i) = [\inf_{v_i \in \mathcal{D}(x_i)} v_i, \sup_{v_i \in \mathcal{D}(x_i)} v_i]$.

A notion of local consistency ϕ is stable under union if for all ϕ-consistent networks $N_1 = \langle \chi, \mathcal{D}_1, \mathcal{C} \rangle$ and $N_2 = \langle \chi, \mathcal{D}_2, \mathcal{C} \rangle$, the network $N' = \langle \chi, \mathcal{D}_1 \cup \mathcal{D}_2, \mathcal{C} \rangle$ is ϕ-consistent. If ϕ is stable under union then for all $N = \langle \chi, \mathcal{D}, \mathcal{C} \rangle, \phi(N) = \langle \chi, \cup\{\mathcal{D}' \subseteq \mathcal{D} | \langle \chi, \mathcal{D}', \mathcal{C} \rangle \text{ is } \phi\text{-consistent}\}, \mathcal{C} \rangle$ is ϕ-consistent and is knows as the ϕ-closure of N. It can be shown that $\phi(N)$ presents the same solutions as N. It can be obtained by iteratively removing the values that do not satisfy ϕ.

3.3. Constraint networks on sets

Some problems involve variables that take subsets of a base set $\mathcal{U}$ as their values. Their domain is then a subset of $\mathcal{P}(\mathcal{U})$, whose cardinality is $2^{|\mathcal{U}|}$. Problems with such domains are generally intractable, and compact representations have therefore been proposed. For instance, the domains can be represented as set intervals [25,47], as follows: $\mathcal{D}(x) = [A, B] = \{E \in \mathcal{P}(\mathcal{U}) | A \subseteq E \subseteq B\}$ with $A, B \in \mathcal{P}(\mathcal{U})$. A constraint C is then said to be bound consistent if $\forall x_i \in vars(C)$,

$$\begin{cases} \cap\{v_i \in \mathcal{D}(x_i)\} = \cap\{v_i \in \mathcal{D}(x_i) | (x_i, v_i) \text{ has a support on } C \text{ in } \mathcal{D}\}, \\ \cup\{v_i \in \mathcal{D}(x_i)\} = \cup\{v_i \in \mathcal{D}(x_i) | (x_i, v_i) \text{ has a support on } C \text{ in } \mathcal{D}\}. \end{cases}$$

This representation is simple and compact, but it has limited representation power. Alternative approximate [24,53] or exact representations [33] have therefore been proposed.

4. Representing the segmentation and recognition problem as a constraint network

In this section, we propose a novel way to express the image interpretation problem. This approach is an original contribution, and in contrast with previous methods, it does not require any prior segmentation of the image to be interpreted.

Let $\mathcal{I} : X \to \mathbb{N}^*$ be an image whose spatial domain X is a subset of $\mathbb{Z}^d$, where d is typically equal to 2 or 3. We wish to obtain regions in X for a set of n objects $\chi = \{O_i | i \in [1 \cdots n]\}$ that are visible in the image; these objects are the variables in our problem. As the image $\mathcal{I}$ provides a discrete view of the continuous world, the regions cannot be represented accurately as subsets of X. The digital sampling and artifacts induced by the acquisition cause imprecision in $\mathcal{I}$ on the object boundaries. We therefore represent the regions as fuzzy subsets of X [62,63]. The variables O_i in our problem are then represented by fuzzy subsets μ_i of X (i.e. $\mu_i : X \to [0,1]$). The set of all fuzzy subsets of X is denoted by $\mathcal{F}$.

The domains $\mathcal{D} = \{\mathcal{D}(A) | A \in \chi\}$ associated with the variables are then subsets of $\mathcal{F}$ ($\mathcal{D}(A) \subseteq \mathcal{F}$). If the problem is satisfiable, then the solutions are among these subsets. An example of the domain for the frontal horn of the left lateral ventricle is displayed in Fig. 2. This small domain contains six fuzzy sets. The third one is the desired solution. However, this domain is not representative of the domains that we typically consider. In fact, the cardinality of $\mathcal{F}$ depends exponentially on $|X|$, and its size is $k^{|X|}$ where k is the number of discrete levels used to represent the membership degrees, and the domains can be any subset of $\mathcal{F}$. We therefore use two bounds to approximate each domain (Section 4.1).

Constraints are obtained from the structural model (see Section 2). For instance, if the model contains the relation "A is to the right of B", then the recognition process must obtain an instantiation $\{(A, \mu_1), (B, \mu_2)\}$, where A and B represent structures of the model, satisfying the constraint $C^{dir}_{A,B}$, i.e. $(\mu_1, \mu_2) \in C^{dir}_{A,B}$. We denote these constraints by $\mathcal{C}$, and their detailed definitions are provided in Section 4.2.

The segmentation and recognition problem is represented by a constraint network $N = \langle \chi, \mathcal{D}, \mathcal{C} \rangle$ and we wish to obtain a solution of N, that is, a consistent instantiation of all variables in χ, that satisfies all of the constraints. We assume that the problem is satisfiable, which means that such a solution exists. In fact, the model presented in Section 2 is designed to be generic and capable of handling normal anatomical variability. However, pathological cases may differ significantly from the normal anatomy, and specialized modeling of the pathologies may therefore be necessary to handle such cases.

The cardinality of the search space is $k^{|X| \times |\chi|}$, where $|X|$ is approximately 10^7 for a typical MRI volume and $|\chi|$ is the number of structures in the model. Clearly, a backtracking algorithm cannot be applied. To obtain a solution, we first simplify the constraint network using a constraint propagation algorithm that removes as many inconsistent values as possible from the domains, according to the constraints. The propagation algorithm obtains the smallest possible element of $\mathcal{P}^{sol}_{ND}$ in polynomial time. For this purpose we propose propagators that are related to each constraint in Section 4.2, and the constraint propa-

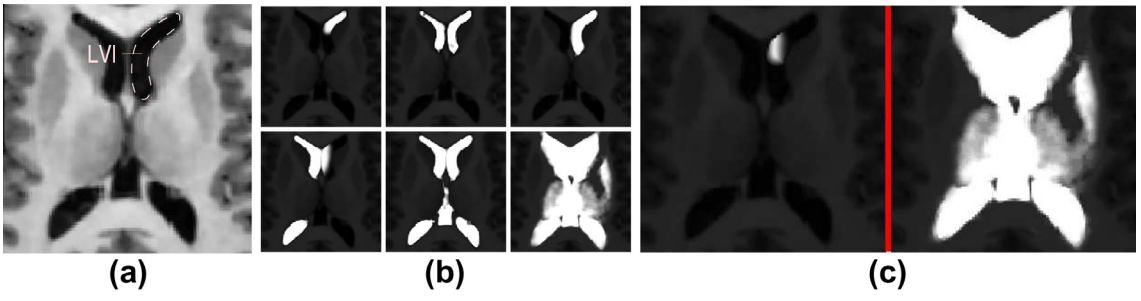

Fig. 2. (a) Axial slice of a brain MRI and outline of the frontal horn of the left lateral ventricle (*LVI*). (b) A domain of *LVI* that contains six fuzzy sets. (c) Lower bound, $\underline{LVI}$, and upper bound, $\overline{LVI}$.

gation algorithm sequentially applies these propagators (Section 4.3). The propagators corresponding to each constraint are described in detail in Section 5.

4.1. Representation of the domains

As the sizes of the domains may vary exponentially with the number of pixels $|X|$, a compact representation is required. In [45], these domains are represented by their minimal bounding boxes. This representation is very compact, but it cannot accurately represent the shapes of the objects, which limits the efficiency of the constraint propagation algorithm.

As mentioned in Section 3, the domains can in some cases be efficiently represented by their bounds, with respect to a partial ordering on the domain. With the usual partial ordering on fuzzy sets,[1] denoted by $\leqslant$, $(\mathcal{F}, \leqslant)$ is a complete lattice. Therefore, every subset of $\mathcal{F}$ has an upper bound and a lower bound that belong to $\mathcal{F}$. The upper bound $\overline{A}$ of the domain $\mathcal{D}(A)$ is therefore defined as follows: $\overline{A} = \bigvee\{v \in \mathcal{D}(A)\}$, where $\forall x \in X,\ \overline{A}(x) = \sup_{v \in \mathcal{D}(A)} v(x)$. This bound is an over-estimation of the target fuzzy set μ_A. Similarly, we define the lower bound $\underline{A}$ as follows: $\underline{A} = \bigwedge\{v \in \mathcal{D}(A)\}$, where $\forall x \in X,\ \underline{A}(x) = \inf_{v \in \mathcal{D}(A)} v(x)$. This bound provides an under-estimation of μ_A.

Definition 1. An interval of fuzzy sets $(\underline{A}, \overline{A})$, defined by a lower bound $\underline{A}$ and an upper bound $\overline{A}$, is the set of elements of $\mathcal{F}$ that lie between these bounds, according to the partial ordering $\leqslant$: $(\underline{A}, \overline{A}) = \{\mu \in \mathcal{F} | \underline{A} \leqslant \mu \leqslant \overline{A}\}$.

If $\underline{A}$ and $\overline{A}$ are the bounds of a given domain $\mathcal{D}(A)$, then the interval $(\underline{A}, \overline{A})$ includes $\mathcal{D}(A)$. As a trivial representation of the domains is not feasible, we represent the domains of our constraint network as intervals. We now write $N = \langle \chi, \mathcal{D}^I, \mathcal{C} \rangle$, where $\mathcal{D}^I$ are domains represented as intervals.

These definitions are illustrated in Fig. 2 for the frontal horn of the left lateral ventricle *LVl* (a). A tiny domain $\mathcal{D}(LVl)$ of *LVl* that contains six values is shown in (b). The bounds of this domain are shown in (c), and we have $\mathcal{D}(LVl) \subseteq (\underline{LVl}, \overline{LVl})$. The representation of a domain by its bounds only is far less accurate than a representation as a subset of $\mathcal{F}$. However, this bounds representation provides a good trade-off between the complexity of the representation and its accuracy.

The constraint propagation algorithm iteratively tightens the domains by computing an increasingly small upper bound and an increasingly large lower bound. If a given domain $(\underline{A}, \overline{A})$ satisfies $\underline{A} \not\leqslant \overline{A}$ during the propagation process, then this domain is empty, and we conclude that the problem is not satisfiable. By convention, an empty interval is represented by $(1_{\mathcal{F}}, 0_{\mathcal{F}})$, where $0_{\mathcal{F}}$ is the least element of $\mathcal{F}$ (a fuzzy set that is equal to 0 everywhere) and $1_{\mathcal{F}}$ is the greatest element (equal to 1 everywhere).

4.2. Definition of the constraints

The constraints are obtained from the structural model. We associate a propagator with each constraint C, i.e. a mapping $f_C : \mathcal{P}^{sol}_{ND} \to \mathcal{P}^{sol}_{ND}$ that tightens the domains by removing values that are inconsistent with respect to C. Because the domains are represented as intervals, we rely on a local consistency criterion, which is weaker than arc consistency, similar to bound set consistency or *bounds*(Z)-consistency.

Definition 2. A constraint C is $\mathcal{BS}_{\mathcal{F}}$-consistent ($\mathcal{BI}_{\mathcal{F}}$-consistent) in $\mathcal{D}^I$ if the upper (lower) bound of the domain of each variable in *vars*(C) can be obtained as the union (intersection) of all of the values in the domain with a support on C in $\mathcal{D}^I$: $\forall A_i \in vars(C)$, $\overline{A_i} = \bigvee\{\mu \in (\underline{A_i}, \overline{A_i}) | (A_i, \mu)$ has a support on C in $\mathcal{D}^I\}$ ($\forall A_i \in vars(C), \underline{A_i} = \bigwedge\{\mu \in (\underline{A_i}, \overline{A_i}) | (A_i, \mu)$ has a support on C in $\mathcal{D}^I\}$). The constraint C is $\mathcal{B}_{\mathcal{F}}$-consistent in $\mathcal{D}^I$ if it is both $\mathcal{BI}_{\mathcal{F}}$-consistent and $\mathcal{BS}_{\mathcal{F}}$-consistent. A constraint network is $\mathcal{B}_{\mathcal{F}}$ ($\mathcal{BS}_{\mathcal{F}}$, $\mathcal{BI}_{\mathcal{F}}$)-consistent if all constraints are $\mathcal{B}_{\mathcal{F}}$ ($\mathcal{BS}_{\mathcal{F}}$,$\mathcal{BI}_{\mathcal{F}}$)-consistent.

The $\mathcal{B}_{\mathcal{F}}$-closure of the initial constraint network $N = \langle \chi, \mathcal{D}^I, \mathcal{C} \rangle$ can be obtained using propagators associated with the constraints. For this purpose, we associate a correct and $\mathcal{B}_{\mathcal{F}}$-consistent propagator f_C with each constraint C.

For any constraint C, we define a generic $\mathcal{B}_{\mathcal{F}}$-consistent propagator f^{gen}_C as follows:

$$f^{gen}_C : \mathcal{P}^{sol}_{ND} \to \mathcal{P}^{sol}_{ND}$$
$$\langle \chi, \mathcal{D}^I, \mathcal{C} \rangle \mapsto \langle \chi, \mathcal{D}^{I'}, \mathcal{C} \rangle,$$

such that $\forall A_i \in vars(C),\ \mathcal{D}^{I'}(A_i) = (\underline{A_i}', \overline{A_i}')$ with:

$$\underline{A_i}' = \bigwedge\{\mu \in (\underline{A_i}, \overline{A_i}) | (A_i, \mu) \text{ has a support on } C \text{ in } \mathcal{D}^I\},$$
$$\overline{A_i}' = \bigvee\{\mu \in (\underline{A_i}, \overline{A_i}) | (A_i, \mu) \text{ has a support on } C \text{ in } \mathcal{D}^I\}.$$

This propagator is not tractable in general. However, for the considered constraints, a simple and computable expression can be derived. In the sequel, a propagator f_C will be described as follows:

$$\frac{\langle vars(C); \mathcal{D}^I; C \rangle}{\langle vars(C); \mathcal{D}^{I'}; C \rangle},$$

[1] Let $\mu, \nu \in \mathcal{F}$, $\mu \leqslant \nu$ if $\forall x \in X$, $\mu(x) \leqslant \nu(x)$.

Data: a network of constraints $\langle \chi, \mathcal{D}^I, \mathcal{C} \rangle$.
a set of propagators $F = \{f_1, \ldots, f_k\}$
Result: $\langle \chi, \mathcal{D}^{I'}, \mathcal{C} \rangle$ $\mathcal{B}_{\mathcal{F}}$-consistent with $\mathcal{D}^{I'} \leq_N \mathcal{D}^I$
Begin
$G \leftarrow F$
While $G \neq \emptyset$ **do**
  select and *remove* a propagator g from G
  if $N \neq g(N)$ **then**
    $G \leftarrow G \cup \{f_i \in F \setminus G \mid vars(f) \cap vars(g) \neq \emptyset\}$
    $N \leftarrow g(N)$
End

Fig. 3. A generic propagation algorithm.

where $\mathcal{D}^I$ and $\mathcal{D}^{I'}$ are the domains associated with the set of variables *vars*(*C*) and $\mathcal{D}^{I'} \leqslant \mathcal{D}^I$.

Before presenting the detailed definitions of the constraints, we briefly describe the constraint propagation process and provide an illustrative example.

4.3. Constraint propagation

The initial network, $N_0 = \langle \chi, \mathcal{D}^I, \mathcal{C} \rangle$, is derived from the structural model. The domains are initialized as $(0_{\mathcal{F}}, 1_{\mathcal{F}})$. If some structures have already been extracted, then the domains of these structures are reduced to singletons, and their upper and lower bounds are then equal.

We calculate the $\mathcal{B}_{\mathcal{F}}$-closure of N_0. This is achieved by iteratively applying the $\mathcal{B}_{\mathcal{F}}$-consistent propagators associated with the constraints. Let $F = \{f_C | f_C$ is $\mathcal{B}_{\mathcal{F}}$-consistent and $C \in \mathcal{C}\}$ be the set of propagators, and let f_C be the function used to compute the $\mathcal{B}_{\mathcal{F}}$-closure of the network $\langle \chi; \mathcal{D}^I; C \rangle$.

As the propagators f_i do not necessarily commute, the propagation is not achieved through a unique application of each propagator but rather through iterative applications of the propagators until convergence is reached. Because the propagators are monotonic, the network obtained at convergence is unique and does not depend on the order of application of the propagators. A generic classical algorithm, belonging to the class *AC*-3, is presented in Fig. 3. Other algorithms could also be used within the proposed framework; what is important and new is the application of the algorithm to well-defined propagators with the required properties, as discussed in the next section. An improvement of this generic algorithm for improved speed is proposed in Section 6.

In the following development, several propagators are defined, some of which are only $\mathcal{BS}_{\mathcal{F}}$-consistent, meaning that they allow only the upper bound to be optimally updated and leave the lower bound generally unchanged. Indeed, we did not obtain cost-efficient $\mathcal{B}_{\mathcal{F}}$-consistent propagators for every constraint. However the constraints are still applied in the proposed algorithm, and the $\mathcal{B}_{\mathcal{F}}$-closure of N_0 is therefore not computed exactly. Practically speaking, the utilized propagators differ from the optimal ones only in very specific cases, and we nearly obtain the $\mathcal{B}_{\mathcal{F}}$-closure. This way to proceed is also relevant for two reasons: (i) we introduce a partition constraint below, and the associated propagator efficiently handles the lower bounds; (ii) the final segmentation algorithm requires mainly the upper bound to be as focused as possible.

Fig. 4 illustrates this algorithm for four variables: the brain (*Br*), left lateral ventricle (*LVl*), left caudate nucleus (*CNl*) and left internal capsule (*ICl*). Initially, no assumptions are made regarding the objects to be recognized. The associated domains are therefore $\mathcal{F}$ and are represented by the bounds $(0_{\mathcal{F}}, 1_{\mathcal{F}})$ (a). In this example, we assume that the brain has already been segmented, as a fuzzy subset μ_{Br}. Its domain is initialized as a singleton and is represented by the bounds (μ_{Br}, μ_{Br}) (b). We then iteratively apply the propagators associated with the constraints (c–j), to gradually update the domains. Each propagator can be applied several times (each time the domain of one of the propagator variables changes, the propagator is added to the list *G* of propagators to update). The process terminates when the network is stable for all of the propagators.

5. Constraint and propagator definitions

This section describes the constraints and associated propagators in detail. The constraints include topological and metric relations, which have been shown to be useful in spatial reasoning [32], and gray level contrasts, which comprise the basic information in the images. These relations are those used by neuro-anatomists to describe the brain, and their interest and usefulness in image recognition has been proved in our previous work based on sequential recognition methods [8,17,23,29]. It is also important that the chosen constraints be representable in the image domain. The set of constraints can of course be expanded, as appropriate for the application.

Our experiments have demonstrated that all of the constraints are useful. Some constraints play specific roles in the reduction of the domains. For instance, the contrast constraint provides the necessary data fidelity term, which makes it possible for the algorithm to run on any specific case. The partition constraint allows the lower bound to be modified, while the other constraints primarily control the upper bound. The connectivity and volume constraints are dealing with the shape information, but they do so in a sufficiently smooth fashion to allow for flexibility in pathological cases (no true shape

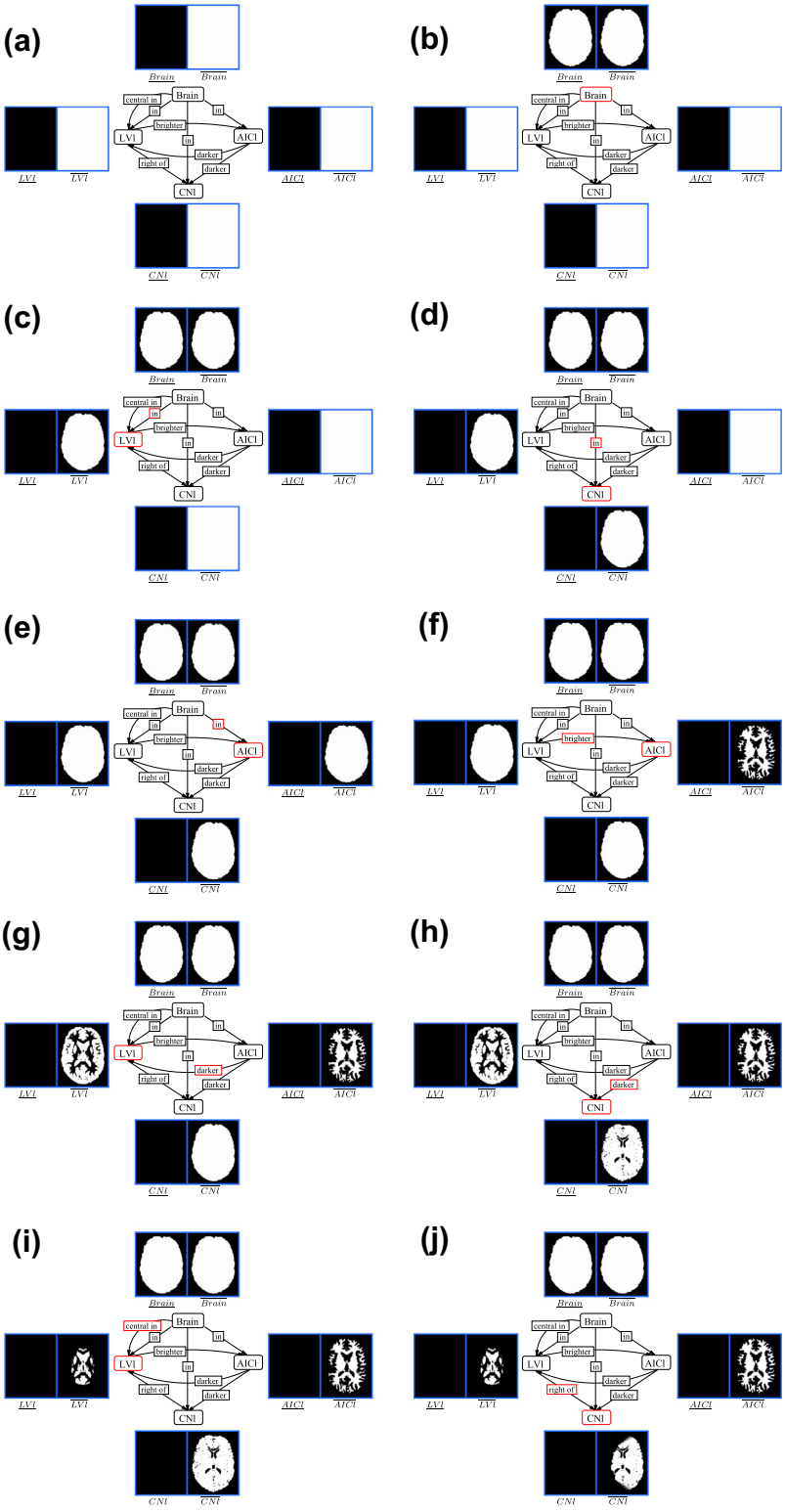

Fig. 4. First iterations of the propagation algorithm.

information is included for this reason). Furthermore, additional constraints can be added to hasten the convergence, such as requiring that all objects be restricted to a bounding box within the brain, thereby reducing the spatial domain to be explored.

For each constraint, we specify the mathematical model and demonstrate the construction of the associated propagator in the sequel. Although the chosen models involve fuzzy sets, the constraints are strict. Proofs of the correction, idempotence and consistency properties of the propagators can be found in [41].

5.1. Definition of the inclusion constraint and associated propagator

An inclusion relation between two structures A and B is satisfied if the region associated with A belongs to the region associated with B. This inclusion relation differs from subsethood measures, as defined in previous studies [13,59]. If the structural model contains an inclusion relation, we add the following constraint to the network.

Definition 3 (*Inclusion constraint*). The constraint $C^{in}_{A,B}$ is associated with the inclusion relation of A in B. This constraint ensures that $vars(C^{in}_{A,B}) = \{A, B\}$ and:

$$C^{in}_{A,B} : \mathcal{D}(A) \times \mathcal{D}(B) \to \{0, 1\}$$
$$(\mu_1, \mu_2) \mapsto \begin{cases} 1 & \text{if } \mu_1 \leqslant \mu_2, \\ 0 & \text{otherwise.} \end{cases}$$

A valid instantiation $I = \{(A, \mu),(B,\nu)\}$ is consistent with respect to $C^{in}_{A,B}$ if $\mu \leqslant \nu$. Conversely, an instantiation that does not satisfy this condition is said to be inconsistent and cannot be extended to a solution. Therefore, a value of $\mathcal{D}(A)$ (or $\mathcal{D}(B)$) that belongs exclusively to inconsistent instantiations cannot belong to a solution. The propagator associated with $C^{in}_{A,B}$ transforms the constraint network by removing as many inconsistent values as possible from $\mathcal{D}(A)$ and $\mathcal{D}(B)$. This removal process reduces the solution space and, in turn, the computational cost of the subsequent decision procedure.

The propagator then updates the bounds of the domains to remove inconsistent values and render $C^{in}_{A,B}\mathcal{B}_{\mathcal{F}}$-consistent. Let us denote the bounds of the set of values of $\mathcal{D}^I(A) = (\underline{A}, \overline{A})$ that are consistent with respect to $C^{in}_{A,B}$ by $\underline{A}_c$ and $\overline{A}_c$: $\{\mu \in (\underline{A}, \overline{A}) | \exists \nu \in (\underline{B}, \overline{B}), C^{in}_{A,B}(\mu, \nu) = 1\}$. The associated propagator must obtain a domain $(\underline{A}', \overline{A}')$ such that $\underline{A} \leqslant \underline{A}' \leqslant \underline{A}_c$ and $\overline{A}_c \leqslant \overline{A}' \leqslant \overline{A}$, with $\underline{A}'$ and $\overline{A}'$ being as close as possible to $\underline{A}_c$ and $\overline{A}_c$. Because we have:

$$\begin{aligned} \overline{A}_c &= \bigvee \{\mu \in (\underline{A}, \overline{A}) | \exists \nu \in (\underline{B}, \overline{B}), \mu \leqslant \nu\} \\ &= \bigvee \{\mu \in (\underline{A}, \overline{A}) | \mu \leqslant \overline{B}\} = \bigvee \{\mu \in \mathcal{F} | \underline{A} \leqslant \mu \leqslant \overline{A} \wedge \overline{B}\} \\ &= \begin{cases} \overline{A} \wedge \overline{B} & \text{if } \underline{A} \leqslant \overline{A} \wedge \overline{B}, \\ 0_{\mathcal{F}} & \text{otherwise,} \end{cases} \end{aligned}$$

$\overline{A}_c$ can be obtained at a low computational cost. We therefore define a propagator that ensures that $\overline{A}' = \overline{A}_c$. Similar updating can be performed on $\underline{B}$ and similar considerations will be used in the sequel to define the propagators associated with other constraints. In this paper, we use $\wedge$ = min and $\vee$ = max because of their idempotence property.

Definition 4 (*Propagator for the inclusion constraint*). The propagator $f_{C^{in}_{A,B}}$ associated with the inclusion constraint of A in B is defined as follows:

$$\frac{\left\langle A, B; (\underline{A}, \overline{A}), (\underline{B}, \overline{B}); C^{in}_{A,B} \right\rangle}{\left\langle A, B; (\underline{A}, \overline{A} \wedge \overline{B}), (\underline{B} \vee \underline{A}, \overline{B}); C^{in}_{A,B} \right\rangle}$$

Proposition 1. *The propagator $f_{C^{in}_{A,B}}$ is correct, idempotent and $\mathcal{B}_{\mathcal{F}}$-consistent.*

The propagator associated with the inclusion constraint $C^{in}_{LVl,Br}$ of the left lateral ventricle (LVl) in the brain (Br) is illustrated in Fig. 5. Initially, $\overline{LVl}$ and $\underline{Br}$ take values of $1_{\mathcal{F}}$ and $0_{\mathcal{F}}$, respectively. The application of the propagator $f_{C^{in}_{LVl,Br}}$ updates both bounds: $\overline{LVl}' = 1_{\mathcal{F}} \wedge \overline{Br} = \overline{Br}$ and $\underline{Br}' = 0_{\mathcal{F}} \vee \underline{LVl} = \underline{LVl}$.

5.2. Directional relative position constraint

To model a directional relation such as "the caudate nucleus (CNl) is exterior to the lateral ventricle (LVl)" (to the right in Fig. 6b), we rely on a fuzzy mathematical morphology approach (see [5] and references therein). For a detailed description of fuzzy mathematical morphology, and the definition and properties of fuzzy dilation in particular, we refer the reader to [6,9], for example. These properties are derived primarily from the underlying complete lattice framework [7,40]. Let us only recall

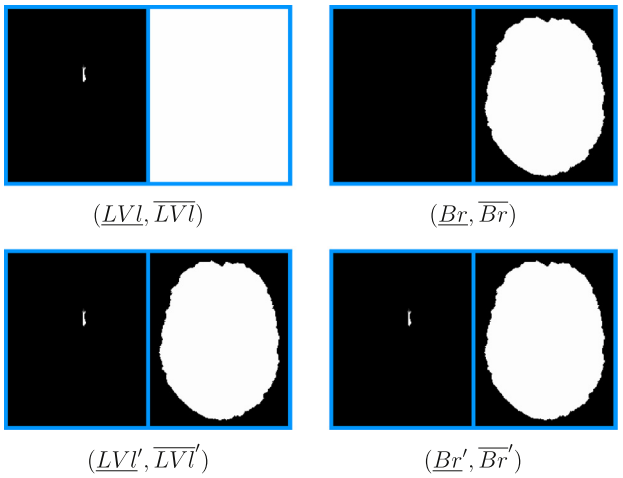

Fig. 5. Illustration of the propagator $f_{C^{in}_{LVl,Br}}$. The domains $(\underline{LVl}, \overline{LVl})$ and $(\underline{Br}, \overline{Br})$ become $(\underline{LVl}', \overline{LVl}')$ and $(\underline{Br}', \overline{Br}')$.

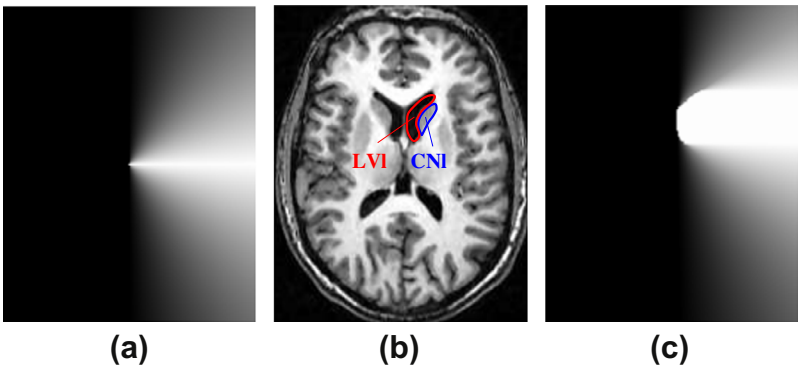

Fig. 6. Illustration of the directional relation "the left caudate nucleus (*CNl*) is to the right of the left lateral ventricle (*LVl*)" on an axial slice (b). (a) Structuring element v associated with the relation. (c) Fuzzy set representing the points to the right of *LVl*.

the definition of the fuzzy dilation of μ by a structuring element v: $\forall x$, $\delta_v(\mu)(x) = \sup_y t(\mu(y), v(x-y))$, where t is a t-norm. In this context, the spatial relation is characterized by a direction $\overrightarrow{u_d}$ and two angles k_1 and k_2 representing the tolerance around $\overrightarrow{u_d}$. With respect to the origin of space, a given point x is in the specified direction with a degree of satisfaction equal to:

$$v(x) = \max\left(0, \min\left(1, \frac{k_2 - \arccos\frac{x \cdot \overrightarrow{u_d}}{\|x\|}}{k_2 - k_1}\right)\right).$$

Fig. 6a depicts the set v for $\overrightarrow{u_d} = \vec{i}, k_1 = 0$ and $k_2 = \frac{\pi}{2}$. The dilation $\delta_v(\mu)(x)$ by the structuring element v then represents the set of points that are in the specified direction with respect to the reference fuzzy set μ. For instance, the fuzzy set in (c) represents all of the points to the right of the lateral ventricle. Note that v can be specified according to the desired semantics of the relation, and other decreasing functions of the angle between x and $\overrightarrow{u_d}$ could be used as well. Finally, two fuzzy sets μ_1 and μ_2 are considered to satisfy the directional relation if $\mu_2 \leqslant \delta_v(\mu_1)$.

Definition 5 (*Directional constraint*). Let A and B be two objects with a stable directional relative position characterized by a structuring element v. The constraint $C^{dirv}_{A,B}$ is defined as follows:

$$C^{dirv}_{A,B} : \mathcal{D}(A) \times \mathcal{D}(B) \to \{0,1\}$$
$$(\mu_1, \mu_2) \mapsto \begin{cases} 1 & \text{if } \mu_2 \leqslant \delta_v(\mu_1), \\ 0 & \text{otherwise.} \end{cases}$$

Definition 6 (*Directional constraint propagator*). The propagator $f_{C^{dirv}_{A,B}}$ that is associated with the directional relative position constraint between two structures A and B is defined as follows:

$$\frac{\langle A, B; (\underline{A}, \overline{A}), (\underline{B}, \overline{B}); C^{dirv}_{A,B} \rangle}{\langle A, B; (\underline{A}, \overline{A}), (\underline{B}, \overline{B} \wedge \delta_v(\overline{A})); C^{dirv}_{A,B} \rangle}$$

Proposition 2. *The propagator $f_{C^{dirv}_{A,B}}$ is correct, idempotent and $\mathcal{BS}_{\mathcal{F}}$-consistent.*

The propagator is only $\mathcal{BS}_{\mathcal{F}}$-consistent because the lower bound of A is not updated, although it could be updated in certain particular cases. However, this updating would require a time-consuming computation for very limited gain.

Fig. 7 illustrates the propagator associated with the relation "*CNl* is to the right of *LVl*". The domain of the caudate nucleus, $(\underline{CNl}, \overline{CNl})$, is reduced by removing elements that do not satisfy the directional relation.

5.3. Distance constraint

We define a distance relation between two structures A and B in an asymmetric fashion, as follows. The distance of all points in region B to region A (represented by μ_A) must fall within a given interval. We represent this interval by a trapezoidal function with parameters d_a, d_b, d_c and d_d (with $0 \leqslant d_a \leqslant d_b \leqslant d_c \leqslant d_d$). The parameters d_a and d_b define a constraint on the minimal distance. With respect to the origin of the space, a point x satisfies this minimal distance relation with degree $c(v_1)(x)$, with $v_1(x) = \min\left(1, \max\left(0, \frac{d_b - \|x\|}{d_b - d_a}\right)\right)$. The complement of the dilation $c(\delta_{v_1}(\mu))$ then represents the set of points that satisfy the minimal distance relation with respect to the reference fuzzy set μ. For the complementation operator c, $c(\alpha) = 1 - \alpha$ ($\forall \alpha \in [0,1]$) can typically be used. Similarly, the parameters d_c and d_d define a constraint on the maximal distance. With respect to the origin, a given point x satisfies this relation with degree $v_2(x) = \max\left(0, \min\left(1, \frac{d_d - \|x\|}{d_d - d_c}\right)\right)$. The dilation $\delta_{v_2}(\mu)$ represents the set of points that satisfy the maximal distance relation with respect to μ.

The set of points contained in the distance interval represented by the trapezoidal function with respect to μ_A can be obtained as follows [5]: $\mu_{Dist}(\mu_A) = c(\delta_{v_1}(\mu_A)) \wedge \delta_{v_2}(\mu_A)$. Finally, the relation between A and B is considered to be satisfied if all of the points of B satisfy the distance relation: $\mu_B \leqslant c(\delta_{v_1}(\mu_A)) \wedge \delta_{v_2}(\mu_A)$.

Definition 7 (*Distance constraint*). Let A and B be two objects satisfying a stable distance relation characterized by the structuring elements v_1 and v_2. The constraint $C^{distv_1v_2}_{A,B}$ can be expressed as follows:

$$C^{distv_1v_2}_{A,B} : \mathcal{D}(A) \times \mathcal{D}(B) \to \{0,1\}$$
$$(\mu_1, \mu_2) \mapsto \begin{cases} 1 & \text{if } \mu_2 \leqslant c(\delta_{v_1}(\mu_1)) \wedge \delta_{v_2}(\mu_1), \\ 0 & \text{otherwise.} \end{cases}$$

Definition 8 (*Propagator for the distance constraint*). The propagator $f_{C^{distv_1v_2}_{A,B}}$ associated with the distance constraint between two structures is defined as follows:

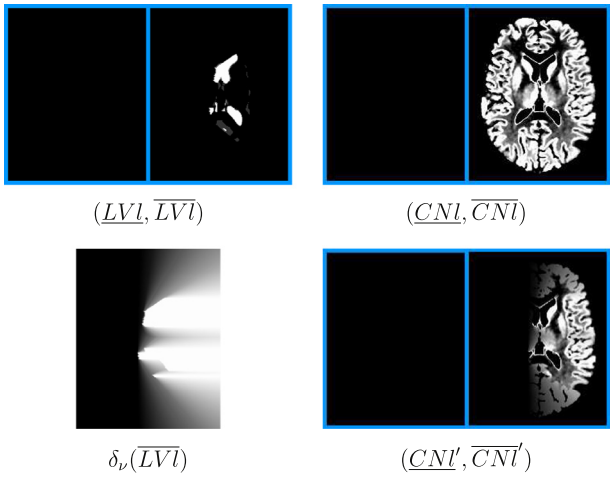

Fig. 7. Illustration of the propagator $f_{C^{dir\ v}_{LVl,CNl}}$, for v as illustrated in Fig. 6. The lower bound of the caudate nucleus domain $\overline{CNl}$ is restricted to the subset of space to the right of the elements of $\mathcal{D}^l(LVl)$ obtained from the dilation $\delta_v(\overline{LVl})$. The resulting upper bound is denoted by $\overline{CNl}'$.

$$\frac{\langle A, B; (\underline{A}, \overline{A}), (\underline{B}, \overline{B}); C_{A,B}^{distv_1v_2} \rangle}{\langle A, B; (\underline{A}, \overline{A} \wedge c(\delta_{v_1}(\underline{B}))), (\underline{B}, \overline{B} \wedge c(\delta_{v_1}(\underline{A})) \wedge \delta_{v_2}(\overline{A})); C_{A,B}^{distv_1v_2} \rangle}$$

The propagator $f_{C_{A,B}^{distv_1v_2}}$ is correct but is neither idempotent nor $\mathcal{BS}_{\mathcal{F}}$-consistent. However, if the minimal and maximal distance constraints are considered independently, then these properties are satisfied. We denote the propagators associated with these constraints by $f_{C_{A,B}^{distminv}}$ and $f_{C_{A,B}^{distmaxv}}$.

Proposition 3. *The propagators $f_{C_{A,B}^{distminv}}$ and $f_{C_{A,B}^{distmaxv}}$ are correct, idempotent and $\mathcal{BS}_{\mathcal{F}}$-consistent.*

As in the case of directional constraints, these propagators are only $\mathcal{BS}_{\mathcal{F}}$-consistent because the lower bounds are not updated, although they could be updated in certain particular situations.

5.4. Partition constraint

The cerebral anatomy can be naturally represented in a hierarchical fashion (Section 2). This hierarchy is encoded in the structural model as partition relations between the anatomical structures. Note that this type of constraint is not restricted to this particular domain but is also applicable in a variety of other fields.

Definition 9 (*Partition constraint*). Consider a set of k structures $\{A_i\}$ and a structure B such that the set $\{A_i\}$ forms a partition of B. The associated constraint is defined as follows:

$$C_{\{A_i\},B}^{part} : \mathcal{D}(A_1) \times \ldots \times \mathcal{D}(B) \to \{0,1\}$$
$$(\mu_1, \ldots, \mu_k, \mu) \mapsto \begin{cases} 1 & \text{if } \mu = \perp_{i\in[1\cdots k]}\mu_i \text{ and } \forall i \neq j, \mu_i \leqslant c(\mu_j), \\ 0 & \text{otherwise}, \end{cases}$$

where $\perp$ is the Lukasiewicz t-conorm, i.e. $\perp(a,b) = \min(1, a+b)$. A review on fuzzy connectives can be found e.g. in [22].

Definition 10 (*Propagator for the partition constraint*). The propagator $f_{C_{\{A_i\},B}^{partition}}$ associated with the partition constraint between the set of structures $\{A_i\}$ and B is defined as follows:

$$\frac{\left\langle \ldots, A_i, \ldots, B; \ldots, (\underline{A_i}, \overline{A_i}), \ldots, (\underline{B}, \overline{B}); C_{\{A_i\},B}^{partition} \right\rangle}{\left\langle \ldots, A_i, \ldots, B; \ldots, \left(\underline{A_i} \vee \top(\underline{B}, c(\perp_{j\neq i}\overline{A_j})), \overline{A_i} \wedge \overline{B} \wedge \bigwedge_{j\neq i} c(\underline{A_j}) \right), \ldots, (\underline{B} \vee \perp_{i\in[1\cdots k]}\underline{A_i}, \overline{B} \wedge \perp_{i\in[1\cdots k]}\overline{A_i}); C_{\{A_i\},B}^{partition} \right\rangle}$$

This propagator is correct, but it is neither idempotent nor $\mathcal{B}_{\mathcal{F}}$-consistent.

Note that the partition propagator updates the lower bounds of all of the involved structures. The partition constraint is essential, in that it is the only constraint that controls the lower bounds other than the inclusion constraint, which has a smaller effect. The use of the partition propagator is therefore highly important, although this propagator has weaker properties.

5.5. Connectivity constraint

Connectivity is an important object characteristic, that is widely used in image interpretation. In fact, the objects considered in image interpretation problems are often connected. In this case, we define a constraint that must be satisfied by the connected regions. Several definitions of fuzzy set connectivity have been proposed, including the definitions of [12,43,49]. We denote the set of fuzzy sets that are connected according to a given definition of connectivity by $\mathcal{H}$ ($\mathcal{H} \subseteq \mathcal{F}$).

Definition 11 (*Connectivity constraint*). Consider a connected object A. The constraint C_A^{conn} is defined as follows:

$$C_A^{conn} : \mathcal{D}(A) \to \{0,1\}$$
$$\mu \mapsto \begin{cases} 1 & \text{if } \mu \in \mathcal{H}, \\ 0 & \text{otherwise}. \end{cases}$$

Definition 12 (*Propagator for the connectivity constraint*). The propagator $f_{C_A^{conn}}$ associated with C_A^{conn} is defined as follows:

$$\frac{\left\langle A; (\underline{A}, \overline{A}); C_A^{conn} \right\rangle}{\left\langle A; (\underline{A}, \xi_{\underline{A}}(\overline{A})); C_A^{conn} \right\rangle}$$

where $\xi_{\underline{A}}(\overline{A}) = \bigvee\{v \in \mathcal{H} | \underline{A} \leqslant v \leqslant \overline{A}\}$.

This propagator is computed by extracting the connected components of $\overline{A}$ based on $\mathcal{H}$, i.e. the greatest elements of $\mathcal{H}$ that are smaller than $\overline{A}$ according to the usual ordering on $\mathcal{F}$. If we denote the set of connected components of $\overline{A}$ by $\mathcal{H}(\overline{A})$, then $\xi_{\underline{A}}(\overline{A})$ can be expressed as $\bigvee\{\mu \in \mathcal{H}(\overline{A}) | \underline{A} \leqslant \mu\}$. Only the connected components including the lower bound are maintained in the result.

The most time-consuming operation in the propagator computation is extracting the connected components. The efficiency of this operation depends on the definition of fuzzy set connectivity. For instance, the extraction of the connected components as defined in [49] can be achieved in quasi-linear time with respect to $|X|$.

Proposition 4. *The propagator $f_{C_A^{conn}}$ is correct, idempotent and $\mathcal{BS}_{\mathcal{F}}$-consistent.*

5.6. Volume constraint

The volume (or surface) of a fuzzy set can be defined as a fuzzy set on $\mathbb{R}^+$ [21], as follows: $f_V(\mu)(v) = \sup_{V(\mu_\alpha) \geqslant v} \alpha$. We represent the prior information regarding the volume by an interval $[f_{V_{\min}}, f_{V_{\max}}]$ where $f_{V_{\min}} : \mathbb{R}^+ \to [0,1]$ and $f_{V_{\max}} : \mathbb{R}^+ \to [0,1]$ represent the minimal and maximal volume, respectively.

Definition 13 (*Volume constraint*). Consider an object A whose volume falls in the interval $[f_{V_{\min}}, f_{V_{\max}}]$. The constraint $C_A^{vol[f_{V_{\min}} f_{V_{\max}}]}$ is defined as follows:

$$C_A^{vol[f_{V_{\min}} f_{V_{\max}}]} : \mathcal{D}(A) \to \{0,1\}$$
$$\mu \mapsto \begin{cases} 1 & \text{if } f_{V_{\min}} \leqslant f_V(\mu) \leqslant f_{V_{\max}}, \\ 0 & \text{otherwise.} \end{cases}$$

Because of the chosen representation of the domains, this constraint is useless when considered alone, as it does not lead to an efficient propagator. However, when the volume constraint is combined with a connectivity constraint, C_A^{conn}, we obtain the following propagator.

Definition 14 (*Propagator for $C_A^{vol[f_{V_{\min}} f_{V_{\max}}]} \wedge C_A^{conn}$*). The propagator $f_{C_A^{vol[f_{V_{\min}} f_{V_{\max}}]} \wedge C_A^{conn}}$ is associated with the conjunction of a volume constraint and a connectivity constraint on the object A. The propagator is defined as follows:

$$\frac{\left\langle A; (\underline{A}, \overline{A}); C_A^{vol[f_{V_{\min}} f_{V_{\max}}]} \wedge C_A^{conn} \right\rangle}{\left\langle A; (\underline{A}, \overline{A}'); C_A^{vol[f_{V_{\min}} f_{V_{\max}}]} \wedge C_A^{conn} \right\rangle}$$

where $\overline{A}' = \bigvee\{\mu \in \mathcal{H} | \underline{A} \leqslant \mu \leqslant \overline{A} \text{ and } f_{V_{\min}} \leqslant f_V(\mu)\}$.

Proposition 5. *The propagator $f_{C_A^{vol[f_{V_{\min}} f_{V_{\max}}]} \wedge C_A^{conn}}$ is correct, idempotent and $\mathcal{BS}_{\mathcal{F}}$-consistent.*

The propagator $f_{C_{LVl}^{vol[f_{V_{\min}} f_{V_{\max}}]} \wedge C_{LVl}^{conn}}$ is illustrated in Fig. 8. This propagator reduces the domain of *LVl* by filtering the connected components of $\overline{LVl}$.

5.7. Adjacency constraint

A measure of adjacency between two fuzzy sets μ_1 and μ_2, denoted by $\mu_{adj}(\mu_1, \mu_2)$, has been proposed in [5]. We adopt this definition in the sequel.

Definition 15 (*Adjacency constraint*). Consider two adjacent objects A and B. We define the constraint $C_{A,B}^{adj}$ as follows:

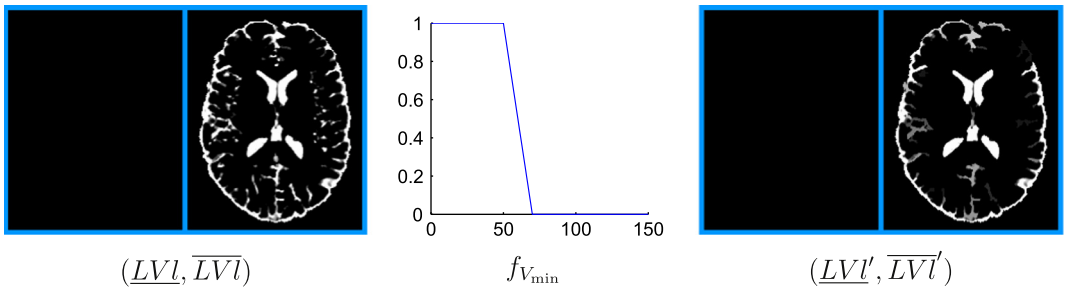

Fig. 8. Illustration of the propagator $f_{C_A^{vol[f_{V_{\min}} f_{V_{\max}}]} \wedge C_A^{conn}}$. The connected components of $\overline{LVl}$ are filtered using a minimal volume criterion.

$$C^{adj}_{A,B} : \mathcal{D}(A) \times \mathcal{D}(B) \to \{0,1\}$$
$$(\mu_1, \mu_2) \mapsto \begin{cases} 1 & \text{if } \mu_{adj}(\mu_1, \mu_2) = 1, \\ 0 & \text{otherwise.} \end{cases}$$

As for the volume constraint, we do not obtain an efficient propagator by considering this constraint alone. We therefore follow the same reasoning as in the previous section and combine the adjacency constraint with a connectivity constraint, C^{conn}_B.

Definition 16 (*Propagator for* $C^{adj}_{A,B} \wedge C^{conn}_B$). The propagator associated with the conjunction of an adjacency constraint between objects A and B and a connectivity constraint on B, denoted by $f_{C^{adj}_{A,B} \wedge C^{conn}_B}$, is defined as follows:

$$\frac{\left\langle A, B; (\underline{A}, \overline{A}), (\underline{B}, \overline{B}); C^{adj}_{A,B} \wedge C^{conn}_B \right\rangle}{\left\langle A, B; (\underline{A}, \overline{A}), (\underline{B}, \overline{B}'); C^{adj}_{A,B} \wedge C^{conn}_B \right\rangle}$$

where $\overline{B}' = \bigvee\{\mu \in \mathcal{H} | \underline{B} \leqslant \mu \leqslant \overline{B} \text{ and } \exists \nu \in (\underline{A}, \overline{A}), \mu_{adj}(\mu, \nu) = 1\}$.

Proposition 6. *The propagator* $f_{C^{adj}_{A,B} \wedge C^{conn}_B}$ *is correct, idempotent and* $\mathcal{BS}_{\mathcal{F}}$*-consistent.*

This propagator can be efficiently computed by extracting the connected components of $\overline{B}$ based on $\mathcal{H}$. The components that are not adjacent to $\overline{A}$ are filtered out. We illustrate the propagator $f_{C^{adj}_{LVl,CNl} \wedge C^{conn}_{CNl}}$ in Fig. 9. The domain bound $\overline{CNl}$ was updated by the propagator because many elements in $(\underline{CNl}, \overline{CNl})$ are either not connected or not adjacent to any element of $(\underline{LVl}, \overline{LVl})$.

5.8. Contrast constraint

Finally, we consider a constraint related to the intensity of the structures to maintain the data fidelity in the propagation process. This constraint is described in detail below for the case of MRI data. Similar constraints can be obtained for other imaging modalities.

As the MRI signal is not normalized, the intensity values of the tissues vary between acquisitions, and it is not appropriate to derive a membership function directly from an example histogram using methods similar to those in [4]. However, for a given acquisition protocol, the contrasts between the structures remain stable. For instance, the lateral ventricles exhibit lower gray level values compared to the white matter. The structural model of the brain therefore includes a set of stable contrast relations.

To model the associated constraint, we associate a membership function $\mu^{\mathcal{I}} : \mathbb{N}^* \to [0,1]$ with each fuzzy set $\mu \in \mathcal{F}$. This membership function represents the gray level values observed in μ in the image $\mathcal{I} : \forall \nu \in \mathbb{N}^*,\ \mu^{\mathcal{I}}(\nu) = \sup_{x \in X, \mathcal{I}(x) = \nu} \mu(x)$. Conversely, a fuzzy set μ' can be obtained from a membership function of the gray levels $\mu'^{\mathcal{I}}$ as follows: $\mu'(x) = \mu'^{\mathcal{I}} \circ \mathcal{I}(x) = \mu'^{\mathcal{I}}(\mathcal{I}(x))$.

We extend Michelson's definition [37] of the contrast κ between two gray levels, ν_1 and ν_2, $(\kappa = \frac{\nu_1 - \nu_2}{\nu_1 + \nu_2})$ to the contrast between two membership functions, ${\mu_1}^{\mathcal{I}}$ and ${\mu_2}^{\mathcal{I}}$. The latter contrast is represented by the membership function $f^{\kappa}_{\mu_1,\mu_2} : [-1,1] \to [0,1]$, as follows: $\forall \nu \in \mathbb{R}, f^{\kappa}_{\mu_1,\mu_2}(\nu) = \sup_{\substack{(\nu_1, \nu_2) \in \mathbb{N}^{*2} \\ \nu = \frac{\nu_1 - \nu_2}{\nu_1 + \nu_2}}} \min\left({\mu_1}^{\mathcal{I}}(\nu_1), {\mu_2}^{\mathcal{I}}(\nu_2)\right)$. If f^{κ} represents the prior information regarding the contrast between μ_1 and μ_2, then we can obtain a membership function ${\mu'_2}^{\mathcal{I}}$ representing gray levels that follow the contrast relation with respect to μ_1: ${\mu'_2}^{\mathcal{I}} = \mu_1^{\mathcal{I}} \times_{\mathcal{N}} f^{k^{-1}}_{\mu_1,\mu_2}$, where:

$(\underline{LVl}, \overline{LVl})$ $(\underline{CNl}, \overline{CNl})$ $(\underline{CNl}', \overline{CNl}')$

Fig. 9. Illustration of the propagator $f_{C^{adj}_{LVl,CNl} \wedge C^{conn}_{CNl}}$. The connected components of $\overline{CNl}$ that are not adjacent to $\overline{LVl}$ are filtered out.

$$\begin{cases} \forall v \in \mathbb{N}^*,\ \mu_1^{\mathcal{I}} \times_{\mathcal{N}} f^{k^{-1}}_{\mu_1,\mu_2}(v) = \sup\limits_{\substack{(v_1,v_2)\in\mathbb{N}^{*2} \\ v = v_1 \times v_2}} \min(\mu_1{}^{\mathcal{I}}(v_1),\ f^{k^{-1}}_{\mu_1,\mu_2}(v_2)), \\ \forall v \in \mathbb{N}^*,\ f^{k^{-1}}_{\mu_1,\mu_2}(v) = \sup\limits_{\substack{u\in\mathbb{R}^{+*} \\ v = \frac{1-u}{1+u}}} f^{\kappa}_{\mu_1,\mu_2}(u). \end{cases}$$

Note that the associated fuzzy set $(\mu_2'^{\mathcal{I}} \circ \mathcal{I})$ is such that $\mu_2 \leqslant \mu_2'^{\mathcal{I}} \circ \mathcal{I}$. Similarly, we define $\mu_1'^{\mathcal{I}}$ as follows: $\mu_1'^{\mathcal{I}} = \mu_2^{\mathcal{I}} \times_{\mathcal{N}} f^k_{\mu_1,\mu_2}$, with $f^k_{\mu_1,\mu_2}(v) = \sup\limits_{\substack{u\in\mathbb{R}^{+*} \\ v = \frac{1+u}{1-u}}} f^{\kappa}_{\mu_1,\mu_2}(u)$. We also have that $\mu_1 \leqslant \mu_1'^{\mathcal{I}} \circ \mathcal{I}$.

We represent the prior information on the contrast between two structures, A and B, by a trapezoidal function $f^{\kappa}(A,B)$ and define the following constraint.

Definition 17 (*Contrast constraint*). Consider two structures, A and B, with a stable contrast represented by a membership function $f^{\kappa}_{A,B}$. The constraint $C^{cont}_{A,B}$ is defined as follows:

$$C^{cont}_{A,B} : \mathcal{D}(A) \times \mathcal{D}(B) \to \{0,1\}$$
$$(\mu_1,\mu_2) \mapsto \begin{cases} 1 & \text{if } \mu_1^l \leqslant \mu_2^l \times_{\mathcal{N}} f^k_{A,B} \text{ and } \mu_2^l \leqslant \mu_1^l \times_{\mathcal{N}} f^{k^{-1}}_{A,B}, \\ 0 & \text{otherwise,} \end{cases}$$

where $\forall v \in \mathbb{N}^+,\ f^{k^{-1}}_{A,B}(v) = \sup\limits_{\substack{u\in\mathbb{R}^{+*} \\ v = \frac{1-u}{1+u}}} f^{\kappa}_{A,B}(u)$ and $\forall v \in \mathbb{N}^+,\ f^k_{A,B}(v) = \sup\limits_{\substack{u\in\mathbb{R}^{+*} \\ v = \frac{1+u}{1-u}}} f^{\kappa}_{A,B}(u)$.

Definition 18 (*Propagator for the contrast constraint*). The propagator $f_{C^{cont}_{A,B}}$ associated with the contrast constraint between two structures A and B is defined as follows:

$$\frac{\left\langle A,B;(\underline{A},\overline{A}),(\underline{B},\overline{B});C^{cont}_{A,B}\right\rangle}{\left\langle A,B;\left(\underline{A},\overline{A}\wedge\left(\mu_{\overline{B}^l}\times_{\mathcal{N}} f^k_{A,B}\circ I\right)\right),\left(\underline{B},\overline{B}\wedge\left(\mu^l_{\overline{A}}\times_{\mathcal{N}} f^{k^{-1}}_{A,B}\circ I\right)\right);C^{cont}_{A,B}\right\rangle}$$

This propagator reduces the upper bounds of the two domains by removing all of the voxels that cannot satisfy the contrast relation. The propagator produces important domain reductions even when the domains are quite large. Indeed, the radiometric membership function of any given domain is limited to the gray levels present in the image.

Proposition 7. *$f_{C^{cont}_{A,B}}$ is correct, idempotent and $\mathcal{BS}_{\mathcal{F}}$-consistent.*

Fig. 10 illustrates these definitions for the contrast constraint between the lateral ventricle (*LVl*) and the caudate nucleus (*CNl*) (b). The associated membership functions $\mu^{\mathcal{I}}_{LVl}$ and $\mu^{\mathcal{I}}_{CNl}$ are depicted in (c). The membership function $f^{\kappa}_{LVl,CNl}$, representing the prior information on the contrast, is shown in (d). We also obtain a membership function (e) representing the intensities satisfying the contrast relation with respect to $\mu_{LVl}\left(\mu^{\mathcal{I}}_{LVl}\times_{\mathcal{N}} f^k_{LVl,CNl}\right)$. If we combine the latter with the image (f), then we can verify that $\mu_{CNl} \leqslant \left(\mu^{\mathcal{I}}_{LVl}\times_{\mathcal{N}} f^k_{LVl,CNl}\right)\circ\mathcal{I}$.

Fig. 11 illustrates the associated propagator. The initial domain $(\underline{LVl},\overline{LVl})$ of the lateral ventricle has previously been reduced, and $(\underline{CNl},\overline{CNl})$ is equal to $(0_{\mathcal{F}},1_{\mathcal{F}})$. We then obtain gray levels that may satisfy the contrast relation with $\mu^{\mathcal{I}}_{\overline{LVl}}$ following $\mu^{\mathcal{I}}_{\overline{LVl}}\times_{\mathcal{N}} f^{k^{-1}}_{LVl,CNl}$. Finally, we deduce the reduced domain $(\underline{CNl}',\overline{CNl}')$.

6. Application to structure recognition in images

In this section, we first incorporate the proposed constraint propagation method into a complete interpretation algorithm. We then provide a demonstration on synthetic examples. Finally, we perform brain structure segmentation and recognition on MR images of healthy subjects, to illustrate the application of the algorithm to real-world data.

6.1. Interpretation process

The interpretation process illustrated in Fig. 1 is based on a structural model that must be constructed beforehand. First, the constraint propagation algorithm proposed in Section 4 is applied. This algorithm provides reduced domains for the target structures, but the final result remains to be extracted. We briefly describe the learning procedure for constructing the model and the final decision process in the following subsections.

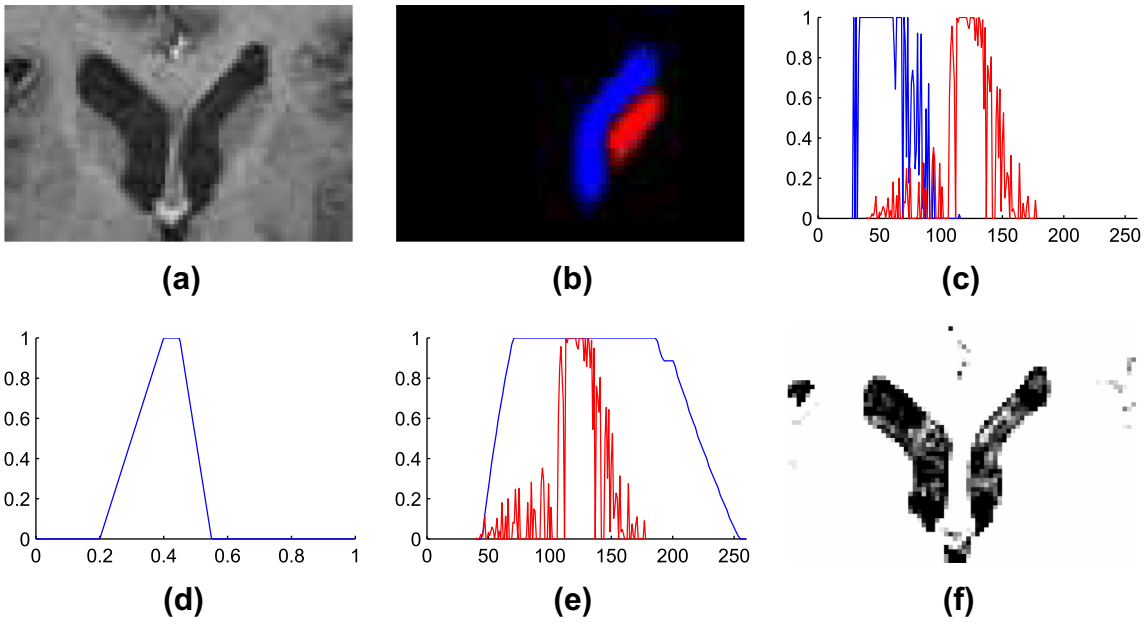

Fig. 10. (a) Cropped axial slice of a 3D MRI volume. (b) μ_{LVl} (blue) and μ_{CNl} (red). (c) $\mu^{\mathcal{I}}_{LVl}$ (blue) and $\mu^{\mathcal{I}}_{CNl}$ (red). (d) Prior information on the contrast between *LVl* and *CNl*: $f^{\kappa}_{LVl,CNl}$. (e) $\mu^{\mathcal{I}}_{CNl}$ (red) and $\mu^{\mathcal{I}}_{LVl} \times_{\mathcal{N}} f^{k}_{LVl,CNl}$ (blue). (f) $\left(\mu^{\mathcal{I}}_{LVl} \times_{\mathcal{N}} f^{k}_{LVl,CNl}\right) \circ \mathcal{I}$. (For interpretation of the references to color in this figure legend, the reader is referred to the web version of this article.)

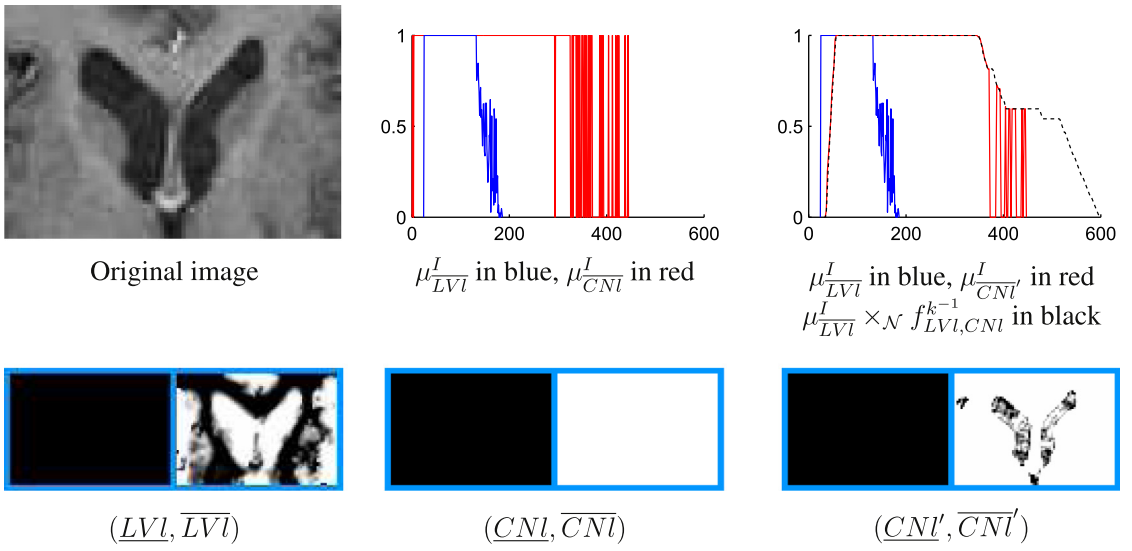

Fig. 11. Illustration of the propagator associated with the contrast constraint between the lateral ventricle (*LVl*) and the caudate nucleus (*CNl*).

6.1.1. Model learning

The model could be constructed manually as an expert system or learned off-line from a set of manually annotated images. The manual method can become very tedious given the large number of brain structures. We therefore decided to design a learning procedure. In the model graph, the vertices are defined as the annotated structures in the learning database, and the model relations (graph edges) are then derived. For this purpose, we check whether all conceivable relations between the structures are satisfied, and retain those relations that are satisfied in all cases. For instance, we evaluate the inclusion of all pairs of structures and add the inclusion relations that are satisfied in all cases to the model. For parameterized relations such as the directional relative positions, we adopt their most restrictive form, provided it covers all cases. For instance, if *A* is strictly to the right of *B* in certain cases, but partially to the right of *B* in other cases, we add the relation obtained in the second configuration (which is satisfied a fortiori in the first case) to the model. Once the model is con-

structed, it is used to interpret all of the images that do not belong to the training database, without requiring any segmentation or annotation of those images.

6.1.2. Extraction of the final result

In general, the constraint propagation algorithm does not reduce the domains to singletons. Even if the domains are strongly reduced, we cannot extract a solution using a backtracking algorithm [26] in all cases because the computation time would be prohibitive. We therefore propose extracting a binary region with a smooth surface that is consistent with the results of the propagation algorithm. This extraction constitutes the final decision-making step.

For a given structure A, we first obtain the fuzzy set $\overline{\partial A}$, which includes the boundary of the structure, from its domain and the domains of adjacent structures. From the model, we obtain the set $Adj(A)$ of structures that are adjacent to A in at least one element of the training set. The boundary of A can then be expressed as the union of the boundaries shared with adjacent structures, $\mu_{\partial A} = \vee_i \mu_{\partial(A,O_i)}$, $O_i \in Adj(A)$, and we can rely on the morphological approach to define the boundary $\mu_{\partial(A,O_i)}$ between A and O_i: $\mu_{\partial(A,O_i)} = \delta_B(\mu_A) \wedge \delta_B(\mu_{O_i})$, where δ_B denotes the dilation by an elementary ball B. Using the results of the propagation, we obtain an overestimation $\overline{\partial A}$ of $\mu_{\partial A}$, as follows: $\mu_{\partial A} \leqslant \bigvee\{\delta_B(\overline{A}) \wedge \delta_B(\overline{O_i}) | O_i \in Adj(A)\}$. Finally, we extract a minimal surface S included in $\overline{A}$ and including $\underline{A}$ by maximizing the following functional:

$$E(S) = \int_{\partial S} \log(\overline{\partial A}(\partial S(s)))ds + \int_S \log(\overline{A}(x))dx + \int_{X\setminus S} \log(c(\underline{A})(x))dx.$$

This functional is efficiently maximized using a graph-cuts algorithm [11]. To obtain a non-empty result, $\underline{A}$ must not be empty. However, this is not always the case. Therefore, we first extract a result for those structures whose inferior boundaries have the highest maximum membership values. We then apply the propagators associated with the partition constraints. If lower bounds are updated, then we iterate the process. In addition, when $\overline{\partial A}$ provides a large overestimation of the boundary, the result may be imprecise. To favor results that more closely match the image boundaries, we add a penalty $\varepsilon(x) = \frac{\epsilon}{(1+\|\nabla \mathcal{I}(x)\|)^2}$:

$$E(S) = \int_{x\in\partial S} (\log(\overline{\partial A}(\partial S(x))) + \varepsilon(x))dx - \int_{x\in S} \log(\overline{A}(x))dx + \int_{x\in X\setminus S} \log(c(\underline{A}(x)))dx,$$

where $\nabla\mathcal{I}$ denotes the image intensity gradient and ϵ is equal to 10^{-2} in the examples presented below.

Although the propagation does not completely solve the problem, it is useful in that it provides lower and upper bounds that are sufficiently close to one another, around the target structure, to enable fast and accurate segmentation. There is typically only one significant image contour in $\overline{\partial A}$ within the search space returned by the propagation algorithm, thus rendering the minimal surface segmentation problem unambiguous. Performing the segmentation directly on the entire image or with weaker constraints would be more difficult, costly, strongly dependent on the initialization, and it would extract the most contrasted structure, that would not necessarily correspond to the desired region. All of these problems are overcame using the constraint propagation. With this propagation method, the minimal surface extraction provides fast and accurate segmentation results.

6.2. Recognition of objects in synthetic images

To illustrate the proposed approach, we have synthesized a set of images including nine objects ($A - I$) whose relative positions and contrasts are quite stable. One element is presented in Fig. 12, and several cases are presented in Fig. 13 to illustrate the variability of the database.

Certain relations, such as the adjacency of G and H, are satisfied in some but not all instances of the database. The parameters of some of the relations also vary. For instance, the relation "B is to the left of F" is strictly satisfied in some cases. In other cases, this relation is satisfied only for larger aperture parameters. In addition, the objects exhibit a Gaussian distribution of intensities whose mean value varies. Nevertheless, the contrast between the structures remains quite stable.

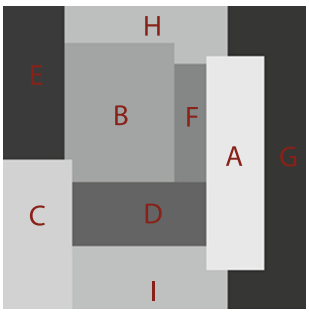

Fig. 12. A synthetic example.

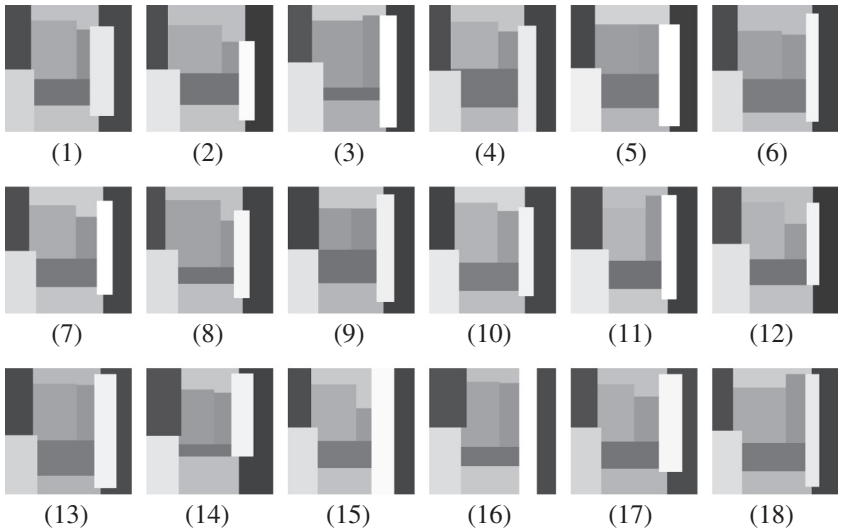

Fig. 13. Synthetic examples.

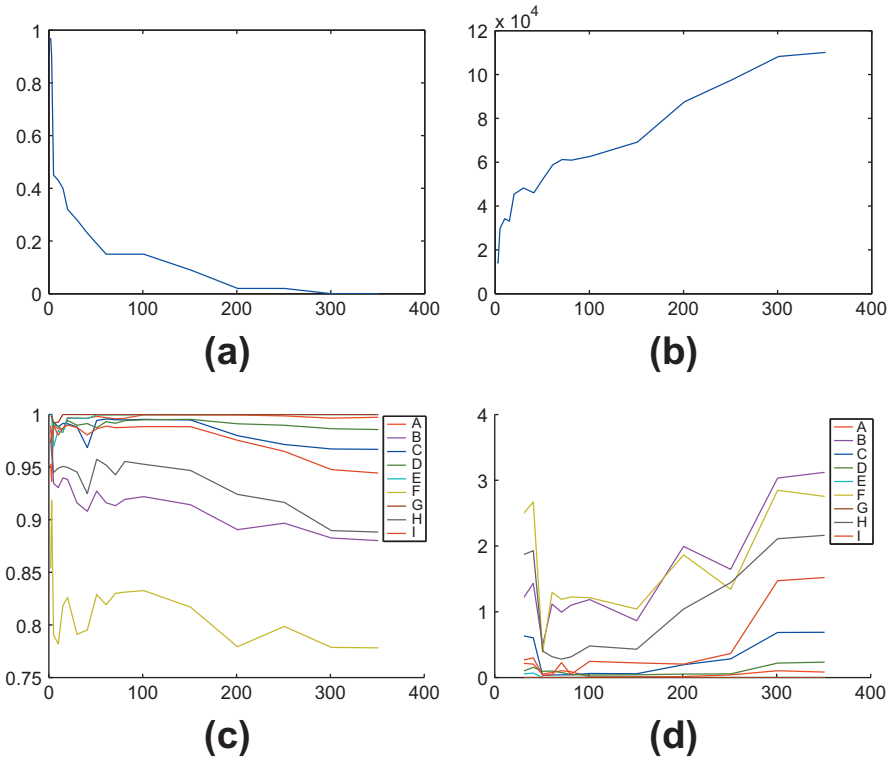

Fig. 14. (a) Proportion of cases for which the propagation process yields inconsistency as a function of the number of cases k used to learn the model. (b) Mean size of the final domains (for the consistent cases). (c) Mean kappa coefficient of the results for the nine structures. (d) Mean distance in pixels between the results and the target regions.

For instance, the gray levels observed in *A* are still much higher than those observed in *G*. Similarly, the gray levels in *B* are higher than those in *F*, although the intensity distributions are nearly equal.

We generate two groups of synthetic examples. The first one contains 350 elements and is used to learn the generic model. The second one contains 100 elements and is used to evaluate the recognition process.

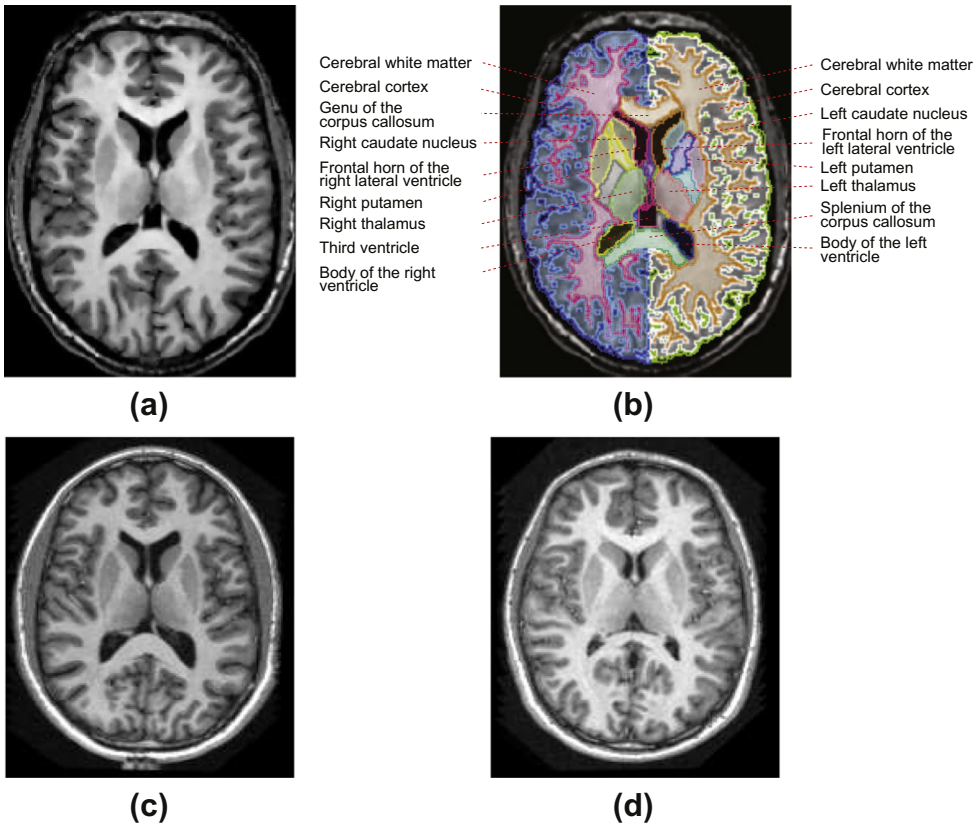

Fig. 15. An instance from the database. (a) Axial slice of a brain MRI. (b) Associated manual outlining. Other cases are shown in (c) and (d).

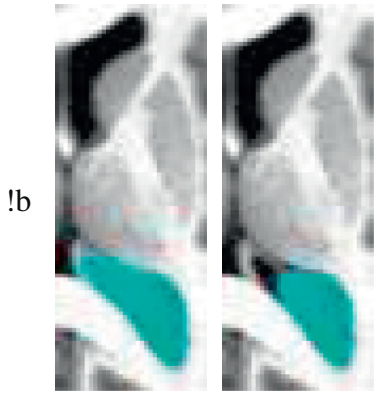

Fig. 16. $\overline{ALVI}$ when the propagation uses G^{s}_{case} (left) versus G^{f}_{case} (right).

6.2.1. Model learning

We first extract the satisfied relations for each instance in the training set, as described briefly in Section 6.1.1. As the relative positions of the nine structures are quite stable, many relations are satisfied in all cases. For instance, *A* and *G* are always adjacent, but *G* and *I* are adjacent only in certain cases (they are not adjacent in the 4th, 15th and 16th cases presented in Fig. 13). In addition, the parameters of certain relations vary, as explained above. For instance, *H* is sometimes strictly to the left of *A*, but in other cases, it is only partially to the left of *A*.

We then merge the relations obtained for the first k cases in the training set. We denote the resulting model by G_k. As k grows, the relations in G_k become less restrictive, but the proportion of cases that are well represented by G_k increases. For instance, if we consider the cases presented in Fig. 13, G_3 contains an adjacency relation between *G* and *I* because the first three cases contain that relation. As the relation is not satisfied in the fourth case, G_k does not contain that relation for $k \geqslant 4$ (which means that *G* and *I* may or may not be adjacent). The relation "*H* is to the left of *A*" is present in G_1 with an aperture

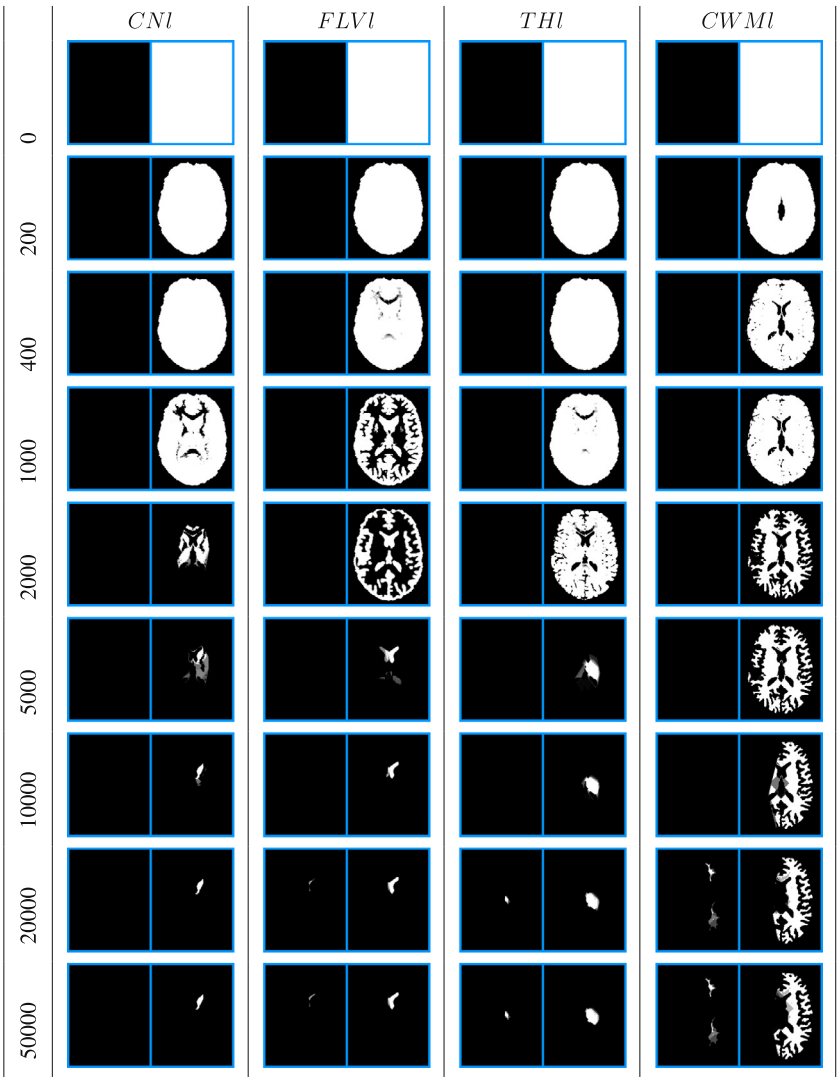

Fig. 17. Evolution of the domains of the left caudate nucleus (*CNl*), frontal horn of the left lateral ventricle (*FLVl*), left thalamus (*THl*) and white matter of the left hemisphere (*CWMl*) during the propagation process.

parameter k_1 equal to 1.12. In G_2, the parameter k_1 is equal to 1.43 and in G_k for $k \geqslant 8$, k_1 is equal to 1.57. Note that the latter is satisfied by all instances in the training set.

6.2.2. Recognition

We use the models G_k (for k between 1 and 350) to perform the recognition of 100 other cases. We initially assign the domain $(0_{\mathcal{F}}, 1_{\mathcal{F}})$ to each structure, and we then apply the constraint propagation algorithm. The algorithm concludes that the problem is inconsistent if G_k does not correctly represent the case under consideration. Fig. 14a shows the proportion of cases in which the algorithm yields inconsistency as a function of the size k of the training set. As k grows, the number of inconsistent cases decreases. However, if more cases are correctly represented, the model becomes weaker and the propagation process yields less domain reduction, as illustrated in Fig. 14b. The mean size of the final domains is presented (for the consistent cases) as a function of the number of cases used in the learning of the model.

We then obtain a binary solution from the resulting domains by extracting a minimal surface (cf Section 6.1.2). We compare the regions obtained for each structure to the target regions using the kappa coefficient $\left(\frac{2|A\cap B|}{|A|+|B|}\right)$, which quantifies the overlap between regions A and B, and the mean distance between the boundaries of A and B. For consistent cases, we present for each structure the mean kappa coefficient (c) and the mean distance (d) with respect to the number of cases used to learn the model in Fig. 14. The results are better for structures that are clearly visible, e.g. A and G, and worse for structures such as F and B, which are not clearly differentiated. However, the kappa coefficient remains higher than 77%, which is generally considered to be a favorable value. The accuracy of the results decreases as k grows. As the propagation algorithm yields larger domains, the model becomes less restrictive.

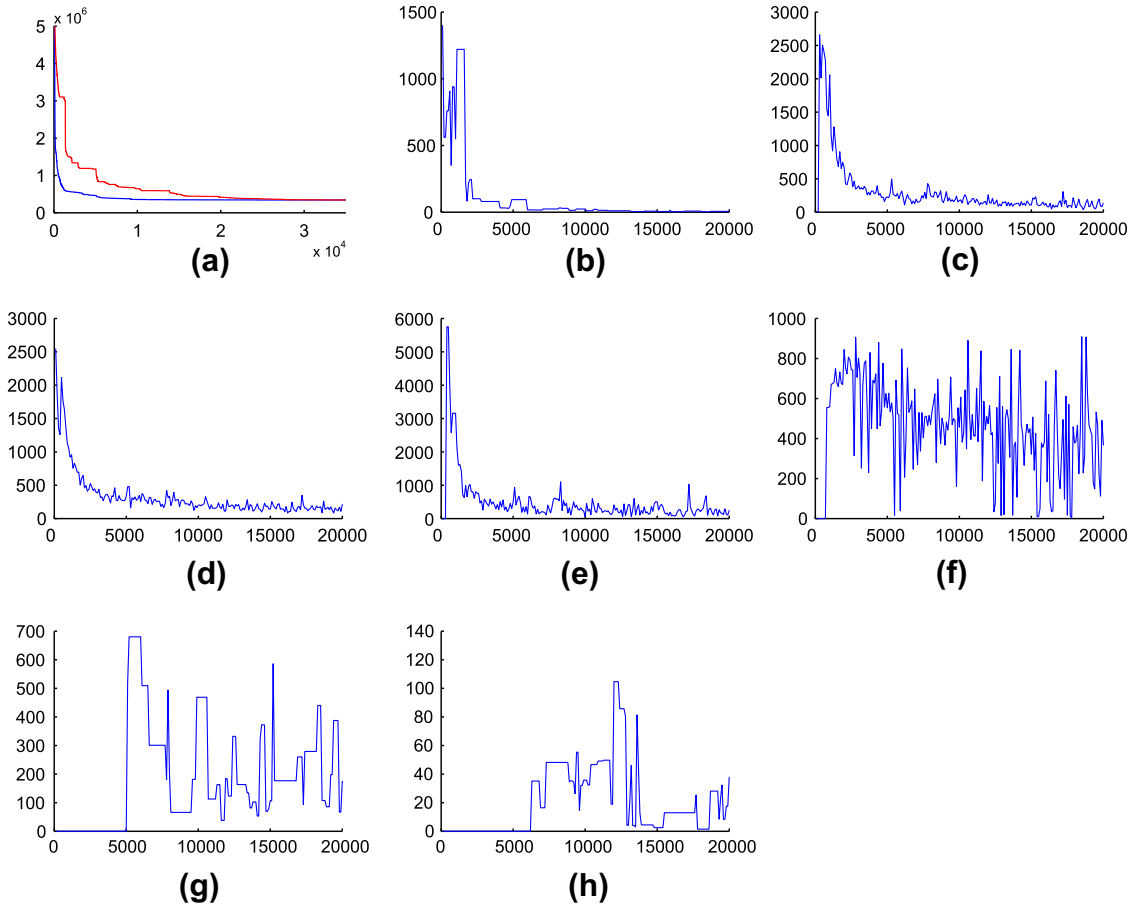

Fig. 18. (a) Evolution of the domain sizes during the constraint propagation for the first case in Fig. 19, using the generic propagation algorithm (red) and a propagation algorithm with specific constraint ordering (blue). Domain reductions achieved by the inclusion (b), direction (c), distance (d), contrast (e), partition (f), connectivity and adjacency (g) and volume (h) constraints as a function of the number of iterations, using the algorithm with constraint ordering. (For interpretation of the references to color in this figure legend, the reader is referred to the web version of this article.)

6.3. Interpretation of brain magnetic resonance images (MRIs)

6.3.1. Brain models

Anatomical models are widely used in the segmentation and recognition of brain structures. These models can be categorized into three main classes: iconic atlases, statistical shape models, and structural models such as graphs, conceptual graphs, ontologies, etc. In this paper we focus on structural models. The structural arrangement of the brain is known and is nearly stable in healthy subjects. Moreover, the structure remains quite stable in the presence of pathologies. This structural arrangement can be encoded as spatial relations of the anatomical structures, as in anatomy textbook descriptions [28,60]. They form a compact representation of the stable properties of the normal anatomy (even if this representation is incomplete), which can be used to perform automatic segmentation and recognition.

6.3.2. Segmentation and recognition of internal brain structures in 2D slices

We have extracted a specific axial slice in six MR volumes from the Oasis database[2] and manually outlined 56 anatomical structures that form a hierarchical representation of the brain in each image, with the root structure representing the entire brain. Two instances from this database are shown in Fig. 15. The relative positions and contrasts of the anatomical structures are quite stable. For instance, the caudate nucleus is always adjacent to the lateral ventricle and is always close to it, although the distance parameters vary. We used several models to evaluate the recognition process, as for the synthetic cases. For each case i in the database we obtain a model denoted by G_i^s. We also obtain model G_i^f based on all instances except for the ith case, and model G^f based on all cases in the data base. These models contain nearly 5000 relations between the 56 structures.

[2] The Oasis database is available at http://www.oasis-brains.org/. It contains MR images acquired on 416 subjects ranging between 18 and 96 years in age. However, these images are not annotated.

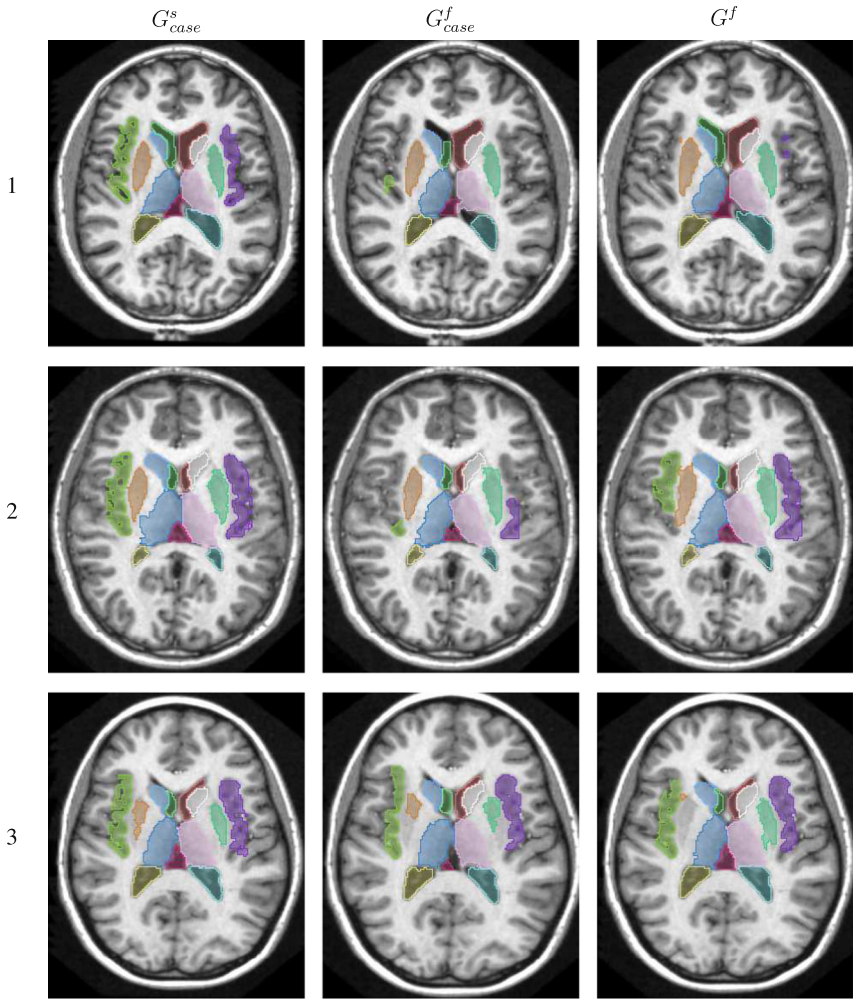

Fig. 19. Final recognition results for the caudate nuclei, lateral ventricles, thalami, putamens, insula lobes and third ventricle for the six cases using models G^s_{case}, G^f_{case} and G^f (see Fig. 15 for the brain structure labels).

We use the three models (G^s_{case}, G^f_{case} and G^f) to evaluate the recognition algorithm for the Oasis database. We first apply the algorithm to each case i using G^s_i, obtained only from that case, to demonstrate the best results that can be obtained using the constraints described in Section 5. We then apply the algorithm to each case i using G^f_i, the model obtained from the other cases. As the training set is relatively small, we also apply the algorithm using G^f, the model obtained from all cases including the case to be recognized. We initialize the recognition process using a preliminary segmentation of the brain surface. This extraction can be performed using existing tools, such as BET [55] or BSE [54]. The domain of the brain is thereby reduced to a singleton, and the other domains are set to $(0_{\mathcal{F}}, 1_{\mathcal{F}})$.

6.3.2.1. Propagation. We apply the constraint propagation algorithm using models G^s_{case}, G^f_{case} and G^f. The algorithm converges after approximately 10,000 to 50,000 iterations.

For a given model G^s_{case}, the algorithm produces tight domains in all cases and never yields inconsistency. In Fig. 17, we illustrate the evolution of the domains of several structures. The upper bounds are increasingly reduced, and, for most structures, they converge to values close to the desired results. However, the lower bounds increase slowly and later over the course of the iterations. In some cases, the lower bounds remain stuck at $0_{\mathcal{F}}$, e.g. for thin structures,[3] thus yielding inaccuracy in the final result.

For a given model G^f_{case}, obtained from all cases except the one that is processed, the process yields inconsistency only in case 5. Although the model was learned from a small number of cases, it clearly exhibits favorable generalization properties.

[3] The lower bounds are generally updated based on partition constraints. To improve the robustness of the propagation algorithm, we use a weakened propagator for partition constraints that erode the lower bound obtained by the original propagator.

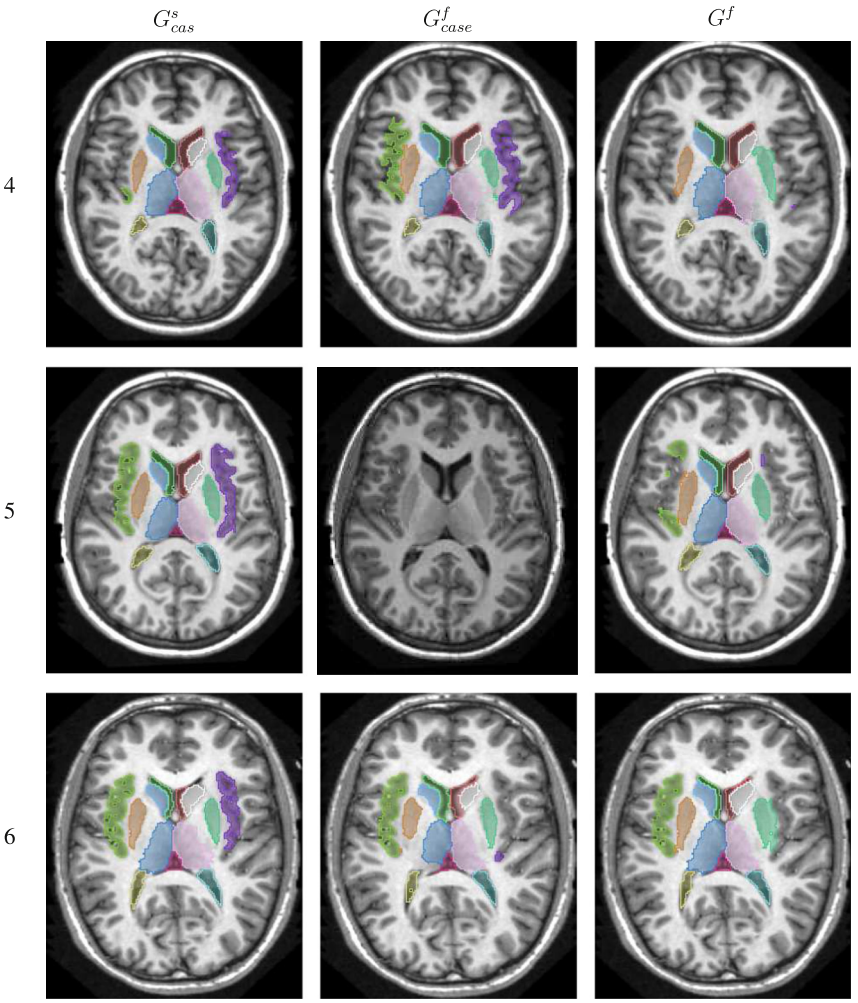

Fig. 20. Continuation of Fig. 19.

Table 1
Mean value of the kappa coefficient, mean distance (D_M) and Hausdorff distance (D_H) between the manual segmentations and the recognition results for the left and right caudate nuclei (*CNl* and *CNr*), frontal horn of the lateral ventricles (*FLVl* and *FLVr*), thalami (*THl* and *THr*), putamens (*PUl* and *PUr*) for the consistent cases using the models G^s_{case}, G^f_{case} or G^f. Distance values are in mm (the image resolution is $1 \times 1 \times 1.25$ mm^3).

Struct	G^s_{case}			G^f_{case}			G^f		
	kappa	D_M	D_H	kappa	D_M	D_H	kappa	D_M	D_H
CDl	0.94	0.3	2.1	0.91	0.5	2.7	0.94	0.3	1.8
CDr	0.94	0.3	2.1	0.91	0.4	2.2	0.94	0.3	1.3
FLVl	0.92	0.5	2.7	0.89	0.4	1.5	0.91	0.4	1.4
FLVr	0.92	0.7	3.2	0.79	2.2	7.8	0.89	0.8	3.4
THl	0.93	0.7	3	0.88	1.2	4.9	0.91	1	4.4
THr	0.93	0.7	2.6	0.87	1.2	4.5	0.92	0.8	3.7
PUl	0.92	0.5	2.9	0.84	1.2	4.9	0.86	1	3.8
PUr	0.91	0.5	2.7	0.82	1.7	6.5	0.73	3	8.5

Consider, for instance, the case illustrated in Fig. 16. The body of the left lateral ventricle (*ALVl*) is close to the mid-sagittal plane, whereas in other cases, it is farther away. Model G^f_1 therefore contains relations that are not satisfied by the target region for *ALVl*, which is not contained in the final domain $(\underline{ALVl}, \overline{ALVl})$. The upper bound $\overline{ALVl}$ (on the right in Fig. 16) can be compared to the upper bound (on the left) obtained using G^s_1.

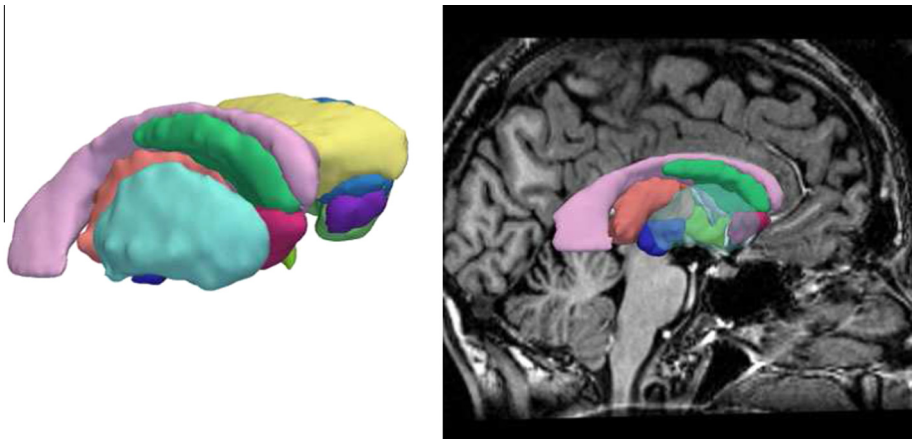

Fig. 21. 3D reconstruction of the recognition results for the caudate nuclei, putamens, lateral ventricles, thalami, third ventricle, accumbens nuclei and subthalami.

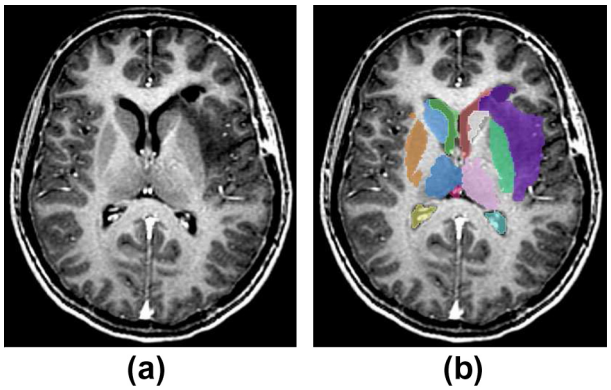

Fig. 22. (a) Axial slice for a subject with a brain tumor. (b) Recognition results for the internal structures and the tumor (purple region). (For interpretation of the references to color in this figure legend, the reader is referred to the web version of this article.)

Finally, we use model G^f (obtained from all cases, including the one being studied) to illustrate the results obtained when the model correctly represents the case under consideration and is less restrictive compared to G^s_{case}.

In Fig. 18, we illustrate the evolution of the domain sizes and the efficiency of the constraints during the propagation algorithm. Using the generic propagation algorithm (see Section 4.3), the domain size initially decreases rapidly and then converges slowly, as shown in red (a). To improve the propagation, we have implemented a constraint ordering algorithm within the generic algorithm. Because the result does not depend on the ordering, we propose several criteria for choosing the next propagator to be computed, including the magnitude of the changes in the domains since the last application of the propagator, the computational cost of the propagator, and a fine estimation of the maximal possible domain reduction. The constraint ordering algorithm enables a significantly more rapid convergence, as illustrated by the blue curve in Fig. 18a. For this algorithm, we also show the domain reductions achieved by the constraints described in Section 5 in (b–h). The largest domain reductions are obtained from the contrast (e), direction (c) and distance (d) constraints. However, all of the constraints contribute to the domain reduction in a complementary manner, and are therefore all useful. For instance, the lower bounds of the domains are updated only by the partition constraints.

6.3.2.2. Extraction of the final solution. Figs. 19 and 20 show the results obtained for the caudate nuclei, lateral ventricles, thalami, putamens, third ventricle and insula for the models G^s_{case}, G^f_{case} and G^f. The segmentation and recognition results are favorable in most cases, and the method therefore provides an effective automated algorithm for interpreting MR images.

To quantitatively evaluate the algorithm, we compare the results to manual segmentations in Table 1. We obtain similar results to those reported in [2]. The best results are obtained using G^s_{case}; in this case, the kappa values are always larger than 0.9, and the mean distances are always smaller than one voxel size. For G^f, the target regions are also contained in the domains obtained using the propagation algorithm. However, these domains are larger, and the final interpretation results are slightly less accurate in some cases, for the left putamen (*PUl*) shown in green, for instance. In addition, the extraction of the right putamen fails completely in the third case; because the resulting lower bound was empty, we were required to update the bound after the final extraction of certain structures, which led to an error. The same problem occurs for model G^f_{case}.

Moreover, the G^f_{case} model does not necessarily correctly represent the case under study, leading to further causes errors. For instance, in the first case, $\overline{ALVI}$ does not fully include the target region, and the final recognition result is incorrect (see Fig. 16). However, this problem occurs rarely.

Overall, a mean error of less than one pixel or voxel was obtained, and the kappa coefficient was larger than 0.8 for G^f_{case}, and even larger for the two other models. These results are very good and promising.

6.3.3. Recognition and segmentation of 3D structures

We now illustrate the application of the algorithm to the entire MRI volume.

Because the computational complexity of the propagators varies at least linearly with the number of pixels, the propagation process becomes very slow in 3D. To reduce the computational cost, we perform the propagator computations on coarser scales if necessary. Certain relations, such as the directional relative positions, exhibit a high level of granularity. The computation of these relations on a subsampled grid does not lead to substantially weaker domain reductions, and the algorithm remains efficient at relatively low computational cost.

Moreover, the ordering of the propagators in the algorithm in Fig. 3 is simple and involves many extraneous computations. We therefore proposed several criteria for choosing the next propagator (the result is independent of the order), as explained previously. This constraint ordering algorithm improves the convergence, and reduces the computation time of the propagation process to a few hours for 3D images.[4] Note that further significant optimizations are still feasible.

Fig. 21 shows a 3D reconstruction of the results obtained for the internal structures.

7. Conclusion

In this paper, we addressed the problem of global scene interpretation based on structural models and proposed a new interpretation method based on a constraint propagation algorithm. The novel aspects of our work include the formulation of the segmentation and recognition problem as a constraint satisfaction problem, without requiring a preliminary segmentation or annotation of the image. A constraint network is constructed from a generic model of the scene, representing its structure through spatial relations between objects and their radiometric contrasts. In addition, we defined constraints based on the relations in the generic model and proposed a specific propagator for each constraint for the first time. We then used a constraint propagation algorithm to reduce the variable domains based on these constraints. Finally, we performed a segmentation of each object based on the tightened domains.

As an illustration, we have applied the proposed framework to the recognition of internal brain structures in MR images, using a model representing the standard neuro-anatomy. Promising results were obtained, with mean errors of less than one voxel size with respect to reference segmentations. There is no inherent methodological or theoretical barrier to 3D application of the method. The only issues are the computational cost and model learning, which requires a large 3D annotated database. Comparisons with other automated methods, in terms of both the accuracy and computation time, should be performed in future experimental studies.

Finally, we comment on the potential extension of the method to pathological cases. Pathologies such as brain tumors can induce large deviations from the normal anatomy and must therefore be considered in the model. In addition, we could allow for the possibility of larger membership functions defining the spatial relations, as proposed in [1]. Fig. 22 illustrates a preliminary result of our extended method. Despite the deformation caused by the tumor, we obtain very good recognition results for the internal structures.

Acknowledgements

This work was partially supported by a grant from the National Cancer Institute (INCA) during Olivier Nempont's PhD work at Telecom ParisTech. We would like to thank Elsa Angelini for her collaboration and support.

References

[1] J. Atif, C. Hudelot, G. Fouquier, I. Fouquier, E. Angelini, From generic knowledge to specific reasoning for medical image interpretation using graph-based representations, in: International Joint Conference on Artificial Intelligence, IJCAI. Hyderabad, India, 2007, pp. 224–229.
[2] K.O. Babalola, B. Patenaude, P. Aljabar, J. Schnabel, D. Kennedy, W. Crum, S. Smith, T. Cootes, M. Jenkinson, D. Rueckert, An evaluation of four automatic methods of segmenting the subcortical structures in the brain, NeuroImage 47 (4) (2009) 1435–1447.
[3] C. Bessière, Constraint Propagation, Tech. Rep., LIRMM, UMR 5506 CNRS, University of Montpellier, 2006.
[4] B. Bharathi Devi, V.V.S. Sarma, Estimation of fuzzy memberships from histograms, Information Sciences 35 (1985) 43–59.
[5] I. Bloch, Fuzzy spatial relationships for image processing and interpretation: a review, Image and Vision Computing 23 (2) (2005) 89–110.
[6] I. Bloch, Duality vs. adjunction for fuzzy mathematical morphology and general form of fuzzy erosions and dilations, Fuzzy Sets and Systems 160 (13) (2009) 1858–1867.
[7] I. Bloch, Lattices of fuzzy sets and bipolar fuzzy sets, and mathematical morphology, Information Sciences 181 (10) (2011) 2002–2015.

[4] This computation time is acceptable when the image analysis is performed in a post-processing stage on a different computer, rather than directly following the image acquisition, thus making other acquisitions possible during the computation time. If automated segmentation and recognition (and derived quantitative measurements) are required, then a few hours is acceptable for the medical experts.

[8] I. Bloch, T. Géraud, H. Maître, Representation and fusion of heterogeneous fuzzy information in the 3d space for model-based structural recognition – application to 3d brain imaging, Artificial Intelligence 148 (1–2) (2003) 141–175.
[9] I. Bloch, H. Maître, Fuzzy mathematical morphologies: a comparative study, Pattern Recognition 28 (9) (1995) 1341–1387.
[10] D. Bowden, R. Martin, Neuronames brain hierarchy, Neuroimage 2 (1) (1995) 63–83.
[11] Y. Boykov, V. Kolmogorov, Computing geodesics and minimal surfaces via graph cuts, International Conference on Computer Vision, ICCV, vol. 1, IEEE, Nice, France, 2003, pp. 26–33.
[12] U. Braga-Neto, J. Goutsias, A theoretical tour of connectivity in image processing and analysis, Journal of Mathematical Imaging and Vision 19 (1) (2003) 5–31.
[13] H. Bustince, V. Mohedano, E. Barrenechea, M. Pagola, Definition and construction of fuzzy DI-subsethood measures, Information Sciences 176 (21) (2006) 3190–3231.
[14] R. Cesar, E. Bengoetxea, I. Bloch, P. Larranaga, Inexact graph matching for model-based recognition: Evaluation and comparison of optimization algorithms, Pattern Recognition 38 (11) (2005) 2099–2113.
[15] C. Choi, W. Harvey, J. Lee, P. Stuckey, Finite domain bounds consistency revisited, Australian Joint Conference on Artificial Intelligence, vol. LNCS 4304, Springer, Hobart, Australia, 2006, pp. 49–58.
[16] O. Colliot, Représentation, évaluation et utilisation de relations spatiales pour l'interprétation d'images, Ph.D. Thesis, Télécom ParisTech, ENST 2003E036, 2003.
[17] O. Colliot, O. Camara, I. Bloch, Integration of fuzzy spatial relations in deformable models – application to brain MRI segmentation, Pattern Recognition 39 (8) (2006) 1401–1414.
[18] D. Conte, P. Foggia, C. Sansone, M. Vento, Thirty years of graph matching in pattern recognition, International Journal of Pattern Recognition and Artificial Intelligence 18 (3) (2004) 265–298.
[19] A. Deruyver, Y. Hodé, Constraint satisfaction problem with bilevel constraint: application to interpretation of over-segmented images, Artificial Intelligence 93 (1–2) (1997) 321–335.
[20] A. Deruyver, Y. Hodé, Qualitative spatial relationships for image interpretation by using a conceptual graph, Image and Vision Computing 27 (7) (2009) 876–886.
[21] D. Dubois, H. Prade, Fuzzy Sets and Systems: Theory and Applications, Academic Press, New York, NY, USA, 1980.
[22] D. Dubois, H. Prade, A review of fuzzy set aggregation connectives, Information Sciences 36 (1-2) (1985) 85–121.
[23] G. Fouquier, J. Atif, I. Bloch, Sequential model-based segmentation and recognition of image structures driven by visual features and spatial relations, Computer Vision and Image Understanding 116 (1) (2012) 146–165.
[24] G. Gange, P. Stuckey, V. Lagoon, Fast set bounds propagation using BDDs, in: European Conference on Artificial Intelligence, ECAI, vol. 178, 2008, Patras, Greece, pp. 505–509.
[25] C. Gervet, Interval propagation to reason about sets: definition and implementation of a practical language, Constraints 1 (3) (1997) 191–244.
[26] S. Golomb, L. Baumert, Backtrack programming, Journal of the ACM 12 (4) (1965) 516–524.
[27] J. Guo, H. Zhou, C. Zhu, Cascaded classification of high resolution remote sensing images using multiple contexts, Information Sciences 221 (2013) 85–97.
[28] D. Hasboun, Neuranat. Université Marie Curie, 2005. <http://www.chups.jussieu.fr/ext/neuranat/index.html>.
[29] C. Hudelot, J. Atif, I. Bloch, Fuzzy spatial relation ontology for image interpretation, Fuzzy Sets and Systems 159 (15) (2008) 1929–1951.
[30] C. Hudelot, J. Atif, O. Nempont, B. Batrancourt, E. Angelini, I. Bloch, GRAFIP: a framework for the representation of healthy and pathological anatomical and functional cerebral information, in: Human Brain Mapping, HBM, Florence, Italy, 2006.
[31] L. Kitchen, Discrete relaxation for matching relational structures, IEEE Transactions on Systems, Man, and Cybernetics 9 (12) (1978) 869–874.
[32] B. Kuipers, T. Levitt, Navigation and mapping in large-scale space, AI Magazine 9 (2) (1988) 25–43.
[33] V. Lagoon, P. Stuckey, Set domain propagation using ROBDDs, Principles and Practice of Constraint Programming, CP, vol. LNCS 3258, Springer, Toronto, Canada, 2004, pp. 347–361.
[34] W. Lin, E. Tsao, C. Chen, Constraint satisfaction neural networks for image segmentation, Pattern Recognition 25 (7) (1992) 679–693.
[35] C. Lipscomb, Medical subject headings (MeSH), Bulletin of the Medical Library Association 88 (3) (2000) 265.
[36] A. Mackworth, Consistency in networks of relations, Artificial Intelligence 8 (1) (1977) 99–118.
[37] A. Michelson, Studies in Optics, Chicago University Press, Chicago, IL, USA, 1927.
[38] R. Mohr, T. Henderson, Arc and path consistency revisited, Artificial Intelligence 28 (2) (1986) 225–233.
[39] U. Montanari, Networks of constraints: fundamental properties and applications to picture processing, Information Sciences 7 (1974) 95–132.
[40] M. Nachtegael, P. Sussner, T. Melange, E. Kerre, On the role of complete lattices in mathematical morphology: from tool to uncertainty model, Information Sciences 181 (10) (2011) 1971–1988.
[41] O. Nempont, Modèles structurels flous et propagation de contraintes pour la segmentation et la reconnaissance d'objets dans les images. Application aux structures normales et pathologiques du cerveau en IRM, Ph.D. Thesis, Télécom ParisTech, ENST 2009E023, 2009.
[42] O. Nempont, J. Atif, E. Angelini, I. Bloch, Structure segmentation and recognition in images guided by structural constraint propagation, in: European Conference on Artificial Intelligence, ECAI, vol. 178, Patras, Greece, 2008, pp. 621–625.
[43] O. Nempont, J. Atif, E. Angelini, I. Bloch, A new fuzzy connectivity measure for fuzzy sets, Journal of Mathematical Imaging and Vision 34 (2) (2009) 107–136.
[44] B. Neumann, R. Möller, On scene interpretation with description logics, Image and Vision Computing 26 (1) (2008) 82–101.
[45] D. Papadias, T. Sellis, Y. Theodoridis, M. Egenhofer, Topological relations in the world of minimum bounding rectangles: a study with r-trees, in: SIGMOD International Conference on Management of Data, ACM Press, San Jose, CA, USA, 1995, pp. 92–103.
[46] A. Perchant, I. Bloch, Fuzzy morphisms between graphs, Fuzzy Sets and Systems 128 (2) (2002) 149–168.
[47] J. Puget, PECOS: a high level constraint programming language, in: Singapore International Conference on Intelligent Systems, SPICIS, vol. 92, Singapore, 1992, pp. 137–142.
[48] N. Ripperda, C. Brenner, Evaluation of structure recognition using labelled facade images, Pattern Recognition 84 (2) (2009) 532–541.
[49] A. Rosenfeld, The fuzzy geometry of image subsets, Pattern Recognition Letters 2 (5) (1984) 311–317.
[50] A. Rosenfeld, R. Hummel, S. Zucker, Scene labeling by relaxation operations, IEEE Transactions on Systems, Man and Cybernetics 6 (6) (1976) 420–433.
[51] C. Rosse, J. Mejino, A reference ontology for bioinformatics: the foundational model of anatomy, Journal of Biomedical Informatics 36 (6) (2003) 478–500.
[52] F. Rossi, P. Van Beek, T. Walsh (Eds.), Handbook of Constraint Programming, Elsevier, New York, NY, USA, 2006.
[53] A. Sadler, C. Gervet, Enhancing set constraint solvers with lexicographic bounds, Journal of Heuristics 14 (1) (2008) 23–67.
[54] D. Shattuck, S. Sandor-Leahy, K. Schaper, D. Rottenberg, R. Leahy, Magnetic resonance image tissue classification using a partial volume model, Neuroimage 13 (5) (2001) 856–876.
[55] S. Smith, Fast robust automated brain extraction, Human Brain Mapping 17 (3) (2002) 143–155.
[56] R. Srihari, Z. Zhang, Show& tell: a semi-automated image annotation system, IEEE Multimedia 7 (3) (2000) 61–71.
[57] Z. Tu, X. Chen, A. Yuille, S. Zhu, Image parsing: Unifying segmentation, detection, and recognition, International Journal of Computer Vision 63 (2) (2005) 113–140.
[58] D. Waltz, Understanding line drawings of scenes with shadows, in: The Psychology of Computer Vision, McGraw-Hill, 1975, pp. 19–91.
[59] C.C. Wang, A modified measure for fuzzy subsethood, Information Sciences 79 (3-4) (1994) 223–232.
[60] S. Waxman, Correlative Neuroanatomy, 24th ed., McGraw-Hill, New York, NY, USA, 2000.

[61] M. Xu, M. Petrou, 3d scene interpretation by combining probability theory and logic: the tower of knowledge, Computer Vision and Image Understanding 115 (11) (2011) 1581–1596.
[62] L.A. Zadeh, Fuzzy sets, Information and Control 8 (3) (1965) 338–353.
[63] L.A. Zadeh, The concept of a linguistic variable and its application to approximate reasoning, Information Sciences 8 (3) (1975) 199–249.
[64] L. Zhang, Z. Zeng, Q. Ji, Probabilistic image modeling with an extended chain graph for human activity recognition and image segmentation, IEEE Transactions on Image Processing 20 (9) (2011) 2401–2413.
[65] S. Zhou, D. Comaniciu, Shape regression machine, International Conference on Information Processing in Medical Imaging, IPMI, vol. LNCS 4584, Springer-Verlag, Kerkrade, The Netherlands, 2007, pp. 13–25.
[66] S. Zhu, D. Mumford, A stochastic grammar of images, Foundations and Trends in Computer Graphics and Vision 2 (4) (2006) 259–362.